



Anisotropic structure of the central North American Craton surrounding the Mid-Continent Rift: Evidence from Rayleigh waves

Anna Foster^{a,b,*}, Fiona Darbyshire^a, Andrew Schaeffer^c

^a Centre GEOTOP, Université du Québec à Montréal, Montréal, QC H2X 3Y7, Canada

^b Now at Yachay Tech University, Hacienda San José S/N, San Miguel de Urquí, Ecuador

^c Geological Survey of Canada, Pacific Geoscience Centre, 9860 West Saanich Road, Sidney, BC, Canada

ARTICLE INFO

2019 MSC:

00-01

99-00

Keywords:

Cratonic lithosphere

Phase velocity

Tomography

Seismic anisotropy

Mantle fabric

Canadian shield

ABSTRACT

The subsurface of the central North American Craton has been imaged by body-, surface-, and full-waveform studies at varying resolutions. These studies offer tantalizing clues about the evolution of Archean and Proterozoic lithosphere. The oldest cratonic lithosphere may have been formed under a different or pre-plate-tectonic regime and, in this region, was later modified by orogenesis around the edges, hotspot passage, rifting and magmatism. We improve the resolution of seismic imaging across the Great Lakes region of North America by carrying out two-station phase velocity dispersion measurements at selected station pairs and inverting them for anisotropic phase velocity maps at periods 20–200 s. We also perform extensive resolution tests to identify robust features in the data. Isotropic features to note are the strong signatures of the Trans-Hudson Orogen, Superior Craton, and Mid-Continent Rift (MCR) at periods most sensitive to the lower crust and uppermost mantle, relatively low velocities near the Great Lakes region at periods most sensitive to the middle lithosphere, and extremely fast velocities in the western Superior at long periods, corresponding to the lowermost cratonic lithosphere. We note a strong contrast in seismic anisotropy across the MCR, with strong anisotropy to the north and weaker anisotropy to the south at shorter periods, consistent with observations from other data types and studies. Fast orientations are heterogeneous within the Superior craton at intermediate periods. At periods ≥ 160 s, an increase in magnitude of the anisotropy, and coherence of the fast orientation, suggest an asthenospheric contribution to the signal.

1. Introduction

The evolution of continental lithosphere is a challenging area of research, with the primary study area being both far beneath the surface and reflecting millions if not billions of years of change. The North American craton is a well-known natural laboratory for these studies, with some of the oldest known crust sitting atop what is inferred to be some of the oldest-known lithosphere. Additionally, while parts of this old lithosphere remain relatively untouched, other parts have been later modified or destroyed by various tectonic processes, including orogeny, rifting, and hotspot passage. This allows us to entertain questions such as whether accreted terranes and blocks bring their own lithosphere with them, which is also accreted, or whether the lithosphere of these smaller terranes is destroyed, and must re-form (e.g., Langford and Morin, 1976; Sol et al., 2002; Canil, 2008; Lee et al., 2011). We can also examine what changes occur at depth with the various modification processes.

The goal of this study is to create high-resolution Rayleigh wave phase-velocity maps with consistent coverage (as much as possible) throughout the study area of central Canada and the north-central United States. This allows comparisons between the structures in different regions, and will provide a strong basis for the inversion of 3-D shear velocity structure in a future study. To this end, we show maps at a range of periods to demonstrate the clear changes that occur in depth in both phase velocity and anisotropy. We also show a variety of resolution tests, to give the reader a sense of how specific features, such as the Superior craton and the Mid-Continent Rift, could be expected to appear in these results.

1.1. Tectonic history

From an earthquake seismology standpoint, cratonic North America is not the most exciting study area; however, from a structural seismology standpoint, there is a lot to see (or not to see, equally as

* Corresponding author.

E-mail address: anna.e.foster@gmail.com (A. Foster).

<https://doi.org/10.1016/j.precamres.2020.105662>

Received 22 November 2019; Received in revised form 10 February 2020; Accepted 11 February 2020

Available online 22 February 2020

0301-9268/ Crown Copyright © 2020 Published by Elsevier B.V. All rights reserved.

interesting). We provide a brief summary of the major tectonic provinces and geologic features in the study area that are of a scale large enough to be significant to surface waves.

1.1.1. Superior craton

The Archean Superior craton, which forms the central core of our study region, is the largest Archean craton preserved on Earth (e.g., [Thurston, 1991](#)). It comprises an assemblage of terranes and domains of continental and oceanic affinity, assembled in the ~3.0–2.6 Ga time period. Detailed overviews of the Superior craton are given by [Percival et al. \(2006\)](#), [Percival \(2007\)](#), [Eaton and Darbyshire \(2010\)](#); here we summarize its main structural features.

In the western and central Superior, terrane boundaries are predominantly oriented in an E–W direction. The core of the western Superior is made up of an amalgamation of two continental blocks of age up to ~3.7 Ga. Craton growth subsequently continued from north to south through a series of accretions, ending with that of another ancient continental block, the Minnesota River Valley Terrane, at ~2.68 Ga. The south-central Superior is dominated by the Abitibi subprovince, which is an assemblage of volcanic and plutonic material and hosts the largest greenstone belt still preserved on Earth. E–W trending terranes make up much of the central and eastern Superior, with the exception of the northeast part of the craton where terrane boundaries rotate to a N–S trend.

The surface geology of the Superior craton is highly varied, including tonalite-trondhjemite-granodiorite (TTG) suites, granites and gneissites, high-grade metamorphic rocks, metasediments and volcanic-plutonic suites thought to be of oceanic affinity. The assemblage of the Superior craton is interpreted by some as the accretion of oceanic and continental terranes via a process similar to that of modern-style plate tectonics (e.g., [Percival et al., 2006](#)), however non-plate-tectonic scenarios have also been proposed for the amalgamation of the craton (e.g., [Bédard and Harris, 2014](#)).

1.1.2. Trans-Hudson Orogen and Hudson Bay

The Trans-Hudson Orogen (THO) is a ~1.8 Ga old Paleoproterozoic orogenic belt that stretches for over 4000 km from the central US into central and northern Canada, linking up with orogenic belts in Greenland and Scandinavia. The orogen marks the destruction of what was likely a > 5000-km-wide ocean, ending with the terminal collision of the Superior craton with the Western Churchill (Rae/Hearne) craton ([Corrigan et al., 2009](#)). Prior to terminal collision, oceanic arcs and continental fragments were accreted to the craton margins. Much of the juvenile Paleoproterozoic material remains well preserved in the wide (> 400 km) orogenic belt, due to (i) the “double-indentor” shape of the edge of the Superior craton, and (ii) the presence of smaller continental blocks, such as the Sask craton, between the Superior and Churchill blocks. The shape, structure and lateral extent of the THO have been compared to that of the modern Himalayan–Tibetan–Karakoram orogen (HKTO) (e.g., [St-Onge et al., 2006](#)).

Hudson Bay is one of four large Paleozoic intracratonic basins in North America, covering a significant portion of the THO with sedimentary sequences and water to depths of ~2.5 km and 100 m respectively. Although the largest basin in terms of surface area, it has the smallest sediment thickness. The relatively minor subsidence is thought to have been controlled by the thick, stiff cratonic lithosphere below the basin. A set of NNW-trending normal faults and a localised uplift in the centre of Hudson Bay divides the basin into two roughly equal sub-basins.

Further details on the Trans-Hudson Orogen and the Hudson Bay basin can be found in the review articles of [Eaton and Darbyshire \(2010\)](#), [Darbyshire et al. \(2017\)](#), and references therein.

1.1.3. Southward growth of Laurentia

Our study area also encompasses a succession of Paleo- to Mesoproterozoic orogenic belts to the south of the Superior craton. The

Penokean orogen deformed the southern margin of the western Superior and accreted oceanic arcs and continental fragments, the largest of which is the Marshfield Terrane in the southern section of the belt. Penokean orogenic activity was coeval with the Trans-Hudson orogen, with deformation and accretion taking place ~1.875–1.835 Ga (e.g., [Whitmeyer and Karlstrom, 2007](#)). Further southward, accretion at the SE Laurentian margin continued with the 1.71–1.68 Ga Yavapai orogeny and the 1.69–1.65 Ga Mazatzal orogeny. Both orogenies sutured oceanic arc terranes and back-arc sequences, and were also associated with volcanic and plutonic events. Further north and east, the Labradorian province of eastern Canada is coeval with the Mazatzal successions, and is characterized by intense metamorphism and plutonism (e.g., [Whitmeyer and Karlstrom, 2007](#)). The southward and eastward growth of Laurentia continued from ~1.55 Ga onwards, with accretion of oceanic arc and back-arc material during the Pinwarian orogeny (1.52–1.46 Ga; [Groulier et al., 2018](#)), and accretion of the Granite-Rhyolite Province. This included an intense period of plutonic activity, which affected all four provinces. The Granite-Rhyolite Province is undeformed in the southeastern section of our study area, but it and the Pinwarian Province were largely overprinted by subsequent tectonic activity leading to the formation of the Grenville orogen (e.g., [Whitmeyer and Karlstrom, 2007](#); [Rivers and Corrigan, 2000](#)).

1.1.4. Grenville Orogen

Between ~1.89 and 1.2 Ga, the southeast Laurentian margin was an active Andean-style margin, with subduction initially directed beneath Laurentia but later reversing polarity. The region was characterized by arc accretion and subsequent widespread magmatism (e.g., [Hynes and Rivers, 2010](#)). Approximately 1.2–1.0 Ga, the Himalayan-scale Grenville orogeny was a key continental collision in the formation of the Rodinia supercontinent. This long-duration, hot orogen had several distinct phases (e.g., [Corrigan and Hanmer, 1997](#); [Hanmer et al., 2000](#); [Rivers, 2015](#) and references therein). Continental collision began on the southeastern margin of the Grenville province at ~1109 Ma, resulting in crustal shortening followed by emplacement of anorthosite, mangerite, charnockite, granite, and related granitoids (AMCG complexes) from 1180 to 1140 Ma. A second cycle followed, with shortening from 1120 to 1090 Ma followed by emplacement of AMCG complexes from 1080 to 1050 Ma ([Corrigan and Hanmer, 1997](#)). This time period overlaps with the “Ottawan phase” (1090–1020 Ma), previously believed to be the initial period of continental collision. Ongoing collision resulted in the formation of a wide plateau similar to the present-day Tibetan plateau, the thrusting of reworked Archean and Proterozoic material onto the Laurentian margin, mid-crustal channel flow and subsequent orogenic collapse ([Rivers, 2015](#)). The later Rigolet phase at 1000–980 Ma primarily affected the NW portion of the orogen, with the bulk of the deformation occurring in the Parautochthonous Belt, including further thrusting, exhumation of the middle and lower crust, and further crustal shortening and thickening. The Grenville Front, which marks the northwestern limit of deformation, was also developed during this orogenic phase. Present-day crustal profiles (e.g., [Ludden and Hynes, 2000](#)) show that Archean basement likely underlies the northwestern parts of the Grenville Orogen up to ~250 km SE of the Grenville Front; however the nature of the boundary in the lithospheric mantle is more complex and less well understood.

1.1.5. Keweenaw Mid-Continent Rift mid-continent rift

The Mid-Continent Rift (MCR) is a ~2000 km long arcuate feature of ~1.1 Ga age, cross-cutting the Archean, Paleo- and Mesoproterozoic tectonic provinces south of the western Superior craton (e.g. [Van Schmus and Hinze, 1985](#); [Sutcliffe, 1991](#); [Ojakangas et al., 2001](#)). Gravity and magnetic maps suggest that its western branch extends at least as far south as Oklahoma, and the east arm extends through Michigan and possibly as far as Alabama (e.g., [Stein et al., 2014](#)). The distinct gravity and magnetic highs associated with the MCR are caused by a large volume (1–2 million km³) of mafic volcanics emplaced in the

rift, and likely the presence of magmatic underplating at the base of the thickened crust. The MCR was traditionally thought to have formed as an isolated intracontinental rift, possibly associated with far-field extension at the time of the Grenville orogeny. However, more recent reinterpretations (Stein et al., 2014) suggest that it formed as a result of plate-boundary reorganization, notably rifting between Laurentia and Amazonia in between compressional phases of the Grenville orogeny. The MCR did not achieve full continental rifting leading to seafloor spreading, but instead ceased extension, leading to subsequent basin inversion and crustal shortening and thickening. The ~20 km thickness of volcanic material emplaced in the MCR suggests that it represents the interaction between a tectonic rift and a mantle plume, leading to flood-basalt volumes comparable to many large igneous provinces (LIP) worldwide (Stein et al., 2015; Stein et al., 2018). Immediately to the north of Lake Superior, the Nipigon Embayment is characterized by significant magmatic influx including diabase sills and flood basalts, with ages similar to those of the magmatic material emplaced in the MCR. The role of the Embayment remains uncertain as it does not exhibit the extensional features characteristic of a (failed) rift arm (Hart and MacDonald, 2007).

1.1.6. Hotspot tectonism

The study region has been affected by various episodes of hotspot-lithosphere interaction throughout its history. The ~2.5 Ga Matachewan mafic dyke swarm covers a large region of the central Superior craton, with dykes radiating in a NNW to NW direction (e.g., Ernst and Bleeker, 2010). A NW–SE trending track of magmatism across eastern Ontario, southwest Quebec and the northeastern US has been attributed to the interaction between the Great Meteor hotspot and the North American lithosphere (Sleep, 1990; Heaman and Kjarsgaard, 2000). The proposed hotspot track is marked by a series of kimberlite eruptions in the Superior craton (~190–150 Ma) and igneous intrusions further to the southeast (e.g., Montegian Hills, ~130–100 Ma), and appears to link up to a chain of seamounts in the NW Atlantic.

1.2. Previous seismic studies

The lithospheric structure of the North American continent has been studied through seismic tomography, receiver function analysis and shear-wave splitting measurements for several decades. Our study region in the center of the continent was relatively poorly resolved in comparison with the tectonically-active western US until the 2010s when the EarthScope USArray Transportable Array (TA) arrived in the central and eastern US. Since that time, a large number of high-resolution models of US lithospheric structure have been published. Data coverage remains more sparse and variable in Canada, however.

1.2.1. Body wave travel time tomography

A series of relative-arrival-time tomographic models was developed between 2007 and 2019 to study the deep structure of the western and central Superior craton, the orogenic belts immediately to its south, and the Mid-Continent Rift (MCR) region, using improvements in data coverage north and south of the Canada/US border to achieve more robust local and regional resolution (Frederiksen et al., 2007; Frederiksen et al., 2013; Bollmann et al., 2019). The most prominent feature imaged in these models is the change from extremely high seismic wave speeds in the Western Superior to relatively lower wave speeds beneath the central Superior of eastern Ontario (Fig. 1). The western edge of the high wave speed region ends ~200 km east of the surface boundary between the Superior and the Trans-Hudson Orogen. In the southwest, the high wave speeds found beneath the Canadian western Superior are divided from those beneath the Minnesota River Valley Terrane by a linear relatively low wave speed feature beneath northern Minnesota and the Dakotas. Other relatively low wave speed anomalies are imaged beneath the western and eastern Penokean syn-taxes and in the shallow lithosphere beneath parts of the western

branch of the MCR. There is no indication of a continuous arcuate anomaly beneath the MCR at the depths resolved by the body wave tomography, however. These features are also visible in USArray-based tomographic models (e.g. Schmandt and Lin, 2014; Burdick et al., 2017; Golos et al., 2018); however these models do not extend north of the Canada/US border in this region. The lower wave speeds in the east of the region appear to be an extension of a prominent low wave speed anomaly that was imaged beneath SE Canada by (e.g.) Rondenay et al. (2000), Villemaire et al. (2012), Boyce et al. (2016). This anomaly has been interpreted to represent lithospheric modification arising from the interaction between the North American continent and the Great Meteor (GM) hotspot.

Boyce et al. (2019) present a model of the North American continent based on absolute travel time tomography. The entire Superior, northeastern Grenville and central-US Archean and Proterozoic terranes exhibit high wave speeds with respect to the global reference, with the exception of the narrow NW-trending low wave speed anomaly previously imaged in SE Canada. This feature appears genuinely slow beneath the Grenville, but transitions to globally fast wave speeds as it enters the Superior. It is the strong contrast with the exceptionally high wave speeds beneath the western Superior that creates the low wave speed anomaly visible in relative arrival time studies.

The lack of a pervasive MCR feature through the mantle lithosphere, and the weakening of the GM anomaly as it reaches the Superior craton, suggest that the Archean lithosphere is more resistant to tectonic modification than the Proterozoic terranes to its south and southeast.

1.2.2. Surface wave and full-waveform tomography

Several studies using two-station Rayleigh wave dispersion measurements and anisotropic tomography have been used to model phase velocity variations, azimuthal anisotropy and shear wave velocity structure in and around our current study area. Darbyshire and Lebedev (2009) found both elevated phase velocities and strong ENE–WSW-oriented anisotropy in the western Superior at all periods studied, with weaker and more variable anisotropy further east. To the north, Darbyshire et al. (2013) imaged lithospheric structure beneath the Hudson Bay region. They found high wave speeds associated with the Superior and Churchill Archean cratonic cores, with a near-vertical band of slightly-lowered wave speeds between them, beneath the Trans-Hudson orogen. The model showed a stratified lithosphere of thickness ~180–280 km, and lithospheric anisotropy patterns suggested extensive deformation related to the Trans-Hudson orogen internides. Petrescu et al. (2017) published phase velocity maps for eastern Canada, showing high wave speeds beneath the Superior, transitioning through intermediate wave speeds beneath the Grenville and slow anomalies beneath the Appalachian domains. The western part of their study, which overlaps with the eastern part of our study, is characterised by WNW–ESE to ENE–WSW trending azimuthal anisotropy. Variation in both phase velocity and azimuthal anisotropy again suggests that the cratonic lithosphere is stratified.

At the continental scale, tomographic models using multi-mode or full-waveform inversions (Yuan et al., 2011; Yuan et al., 2014; Schaeffer and Lebedev, 2014) show a thick (~200–250 km), high wave speed lithospheric root underlying the entire North American craton. Localised anomalies with relatively lower wave speeds are visible beneath parts of the Trans-Hudson orogen, the Mid-Continent rift region, the eastern Penokean orogenic belt and SE Canada. In the model of Yuan et al. (2014), MCR-related anomalies are restricted to depths of 70 km, whereas Schaeffer and Lebedev (2014) model a more pervasive “hole” in the high wave speed core beneath this region. The model of Yuan et al. (2011) included both radial and azimuthal anisotropy. Variations in anisotropy with depth were used to interpret a stratified lithosphere with two distinct layers beneath the North American craton.

Data from the USArray TA were used in surface wave tomography to image the crust and uppermost mantle of the MCR region and the continental US as a whole (Shen et al., 2013; Shen and Ritzwoller,

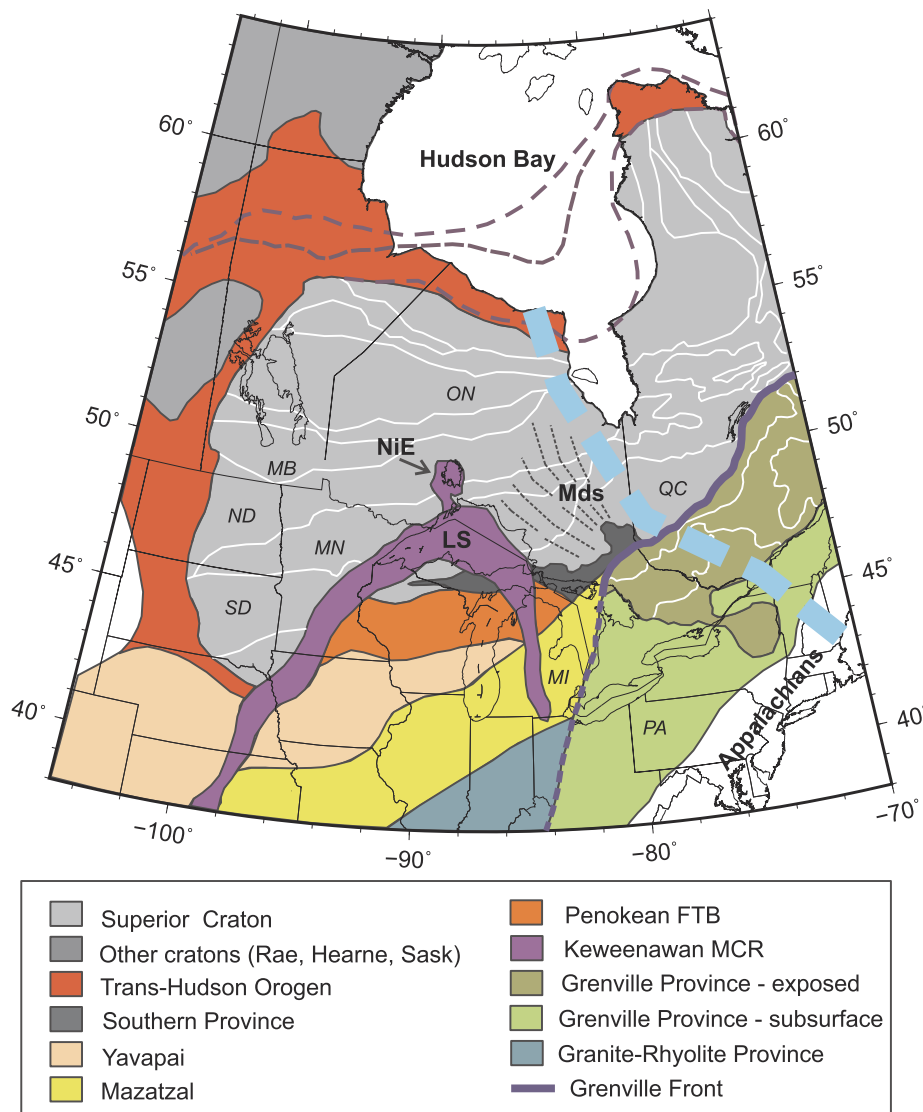


Fig. 1. Main tectonic provinces in the study area, modified from Whitmeyer and Karlstrom (2007), Clowes (2010), Rivers (2015). FTB: fold-and-thrust belt, NiE: Nipigon Embayment, LS: Lake Superior, Mds: Matachewan dyke swarm (after Ernst and Bleeker (2010)). States/provinces mentioned in the text are labeled. ON: Ontario, QC: Quebec, MB: Manitoba, ND, SD: North and South Dakota, MN: Minnesota, MI: Michigan, PA: Pennsylvania. The turquoise dashed line is the approximate track of the Great Meteor hotspot (Heaman and Kjarsgaard, 2000).

2016). Group and phase velocity maps show low wave speed anomalies associated with the MCR, particularly its western branch, at short to intermediate periods. In the resulting shear wave speed models, the western MCR is clearly imaged as a relatively continuous low wave speed anomaly in the upper crust, but the anomalies become more patchy and less clearly correlated with the MCR at depth. The MCR is also associated with anomalously thick crust, with Moho depths of over 50 km in places along the rift. This feature was also seen by Zhang et al. (2016) in a detailed receiver function study of the western MCR, along with a distinct anomalous layer at the base of the crust that was attributed to mafic underplating of the rift.

1.2.3. Shear wave splitting

Seismic anisotropy has been extensively studied in the central and western Superior by a number of studies using permanent and temporary seismograph installations (e.g. Silver and Kaneshima, 1993; Kay et al., 1999; Frederiksen et al., 2007; Frederiksen et al., 2013; Ola et al., 2016). While shear wave splitting provides limited direct information on the depth extent of seismic anisotropy, lateral variations between neighbouring stations may be used to estimate its source through

Fresnel-zone arguments. Shear wave splitting parameters are highly variable across the Superior, Penokean and MCR region. In particular, the western Superior is characterised by very strong splitting, whereas regions further east and south exhibit weaker splitting, with average delay times roughly half of those in the western Superior (Frederiksen et al., 2007). Localized zones of very weak splitting were interpreted by Ola et al. (2016) as arising from MCR-related lithospheric modification. Fast-polarisation orientations in the western Superior range from almost E–W on its eastern side to almost NE–SW in the southwest, showing a gradual rotation westwards. In contrast, splitting parameters measured close to the Trans-Hudson borderlands showed a fast-orientation parallel to the tectonic boundary.

The significant variation in splitting delay times and the correlation between fast-orientations and surface tectonic boundaries led Frederiksen et al. (2007), Frederiksen et al. (2013), and Ola et al. (2016) to propose a dominantly lithospheric contribution to the observed seismic anisotropy. In contrast, Yang et al. (2014) and Yang et al. (2017) proposed that most of the anisotropy could be explained by lithosphere-asthenosphere coupling and present-day sublithospheric mantle flow, based on splitting measurements made for the ensemble of

USArray TA stations in the central and eastern US. Regional-scale surface wave tomography will likely help to resolve this discrepancy, as it allows constraint of the depth of azimuthal anisotropy.

2. Methods

In order to focus our study on the region of interest, we use a two-station method to remove source and teleseismic path effects from the dispersion measurements (e.g., Knopoff et al., 1966; Yao et al., 2006; Foster et al., 2014). We make measurements of the average phase velocity along an inter-station path for a given earthquake and station pair; by choosing to use an event-based method as opposed to ambient noise two-station methods, we are prioritizing deeper structure (longer periods) over the upper crust (shorter periods). Many different multi-station methods have been successfully applied to regional studies (e.g., Sato, 1955; Brune and Dorman, 1963; Gombert et al., 1988; Friederich, 1998; Forsyth and Li, 2005; Bourova et al., 2005; Liang and Langston, 2009; Lin et al., 2009); because measurements using the method of Meier and Dietrich (2004) have already been used in neighboring regions of Canada (Darbyshire and Lebedev, 2009; Darbyshire et al., 2013; Petrescu et al., 2017), we also use this method. This will allow more meaningful comparisons between observed structures, particularly those that may extend across study boundaries.

The key steps of the method are as follows:

- Select station pairs that meet the desired criteria for a given earthquake, where the event-station back-azimuth should lie within $\pm 5^\circ$ of the interstation back-azimuth.
- Standardize the instrument response.
- Cross-correlate the vertical component, and filter to reduce side lobes.
- Transform the cross-correlation function to the frequency domain, and calculate the non-unique inter-station frequency-dependent phase velocity solutions.
- Manually select the appropriate solution branch, based on comparisons with regional and global average dispersion curves, and the appropriate period range, based on the power at different frequencies in the original seismograms and the correlation function. This produces the final inter-station dispersion curve for that earthquake and station pair.
- Average all dispersion curves for a given station pair, to reduce the effects of off-path structure.

Details of the method can be found in Meier and Dietrich (2004) and Petrescu et al. (2017).

3. Data and analysis

3.1. Selected stations and waveform data

Seismic imaging in the area of interest in this study has traditionally been plagued by data inequalities crossing the US-Canada border. With the availability of USArray Transportable Array (TA) data in the US and limited parts of southernmost Canada, this is still a factor. However, by selecting stations from a variety of available networks in Canada over more than a decade, we can obtain fairly even coverage with station spacing of approximately 200 km. We select TA stations with similar spacing in the US, prioritizing those stations that later remained in place as part of the N4 network to maximize the time of station operation. Finally, we add stations around the edge of the area with slightly greater inter-station spacing, roughly 300–600 km, to reduce edge effects in the area of interest, for a total of 69 stations (Fig. 2). Waveforms for global earthquakes between January 2005 and August 2016, with magnitude greater than Mw 6 and epicentral distance greater than 20° , were obtained from the IRIS Data Management Center (DMC) and the Canadian Hazards Information Service, Natural

Resources Canada, totaling 1405 events.

3.2. Two-station measurements

Two-station measurements are made for all earthquakes and station pairs with an inter-station distance ≥ 300 km, and a difference in back-azimuth between station pairs and station-event great-circle paths of less than 5° . The period range for each measurement varied, typically covering some portion of the 20–220 s range. Multiple dispersion measurements for a station pair are averaged to produce a single dispersion curve. This resulted in 815–1309 averaged measurements at any given period.

The sensitivity of surface waves to 3-D velocity structure is an integral over a depth range, the details of which depend on the frequency of the wave. As such, a dispersion curve is expected to be smooth. Some methods impose this requirement during the dispersion picking. In this study, we impose this condition afterwards by fitting a smooth curve (corresponding to a smooth Earth model) to the picked dispersion measurements in SURF96 (Herrmann, 2013), with a high tolerance for misfit on outliers. We then treat this smoothed curve as the final data.

Lastly, we choose to exclude paths that exceed a specified proportion of the measurement error, to remove poor quality measurements. After testing a variety of different thresholds for exclusion, ranging from 0.6 to $2.0 \times \text{error}$, we find that including more paths does not cause significant changes in the distribution of the resulting isotropic or anisotropic velocity anomalies at most periods, and does not change the average phase velocity of each model. It does typically increase the strength of isotropic velocity anomalies, and hence the roughness of the resulting model. We therefore view the higher threshold as more appropriate, and set the limit as 2 times the measurement error. This retains 73–86% of the data at 20–35 s period, 92–95% of the data at 40–60 s period, and 97–99% of the data at longer periods.

3.3. Inversion set-up and regularization

The averaged, smoothed dispersion measurements are inverted for phase velocity maps at discrete periods, by solving a linearised least-squares inversion on a triangular model grid (Lebedev and van der Hilst, 2008; Wang and Dahlen, 1995). We solve for isotropic phase velocity, 2ψ anisotropy, and 4ψ anisotropy (Paige and Saunders, 1982; Smith and Dahlen, 1973). Rayleigh waves have very little sensitivity to 4ψ anisotropy in the mantle (e.g. Montagner and Anderson, 1989), and we do not interpret those results, but they are included in the solution for completeness. Inversion parameters that must be set by the user include grid size, smoothing, and damping values. Inter-station path lengths range from 300 to 2500 km, with most paths falling in the 300–1500 km range. Based on this distribution and on the average spacing of seismic stations across the study region, the grid node spacing is selected as 150 km or half of the minimum inter-station distance.

Smoothing and damping values for the inversion, for both isotropic and anisotropic heterogeneity, are subjectively chosen based on a number of tests. The bulk of the parameter testing was carried out at three periods with varying path coverage (Fig. 3): 30 s (1216 paths), 75 s (1308 paths), and 180 s (966 paths). The best path coverage (1200 or more paths) is at 30–100 s period. The most sparse path coverage is at 200–220 s period, with fewer than 900 paths.

Tests to find the best approximate smoothing values were conducted with damping held constant at a low value of 0.05. Initially, we examined the effect of varied isotropic and anisotropic smoothing on roughness versus remaining variance curves. Both the isotropic and anisotropic smoothing curves exhibit the expected shape of a trade-off curve, making it possible to select a range of smoothing parameters corresponding to the ‘knee’ of the curve, or the optimal trade-off between roughness and variance reduction. This range was then inspected visually, and approximate best smoothing values were chosen. Similar tests to find the best approximate damping values were carried out with

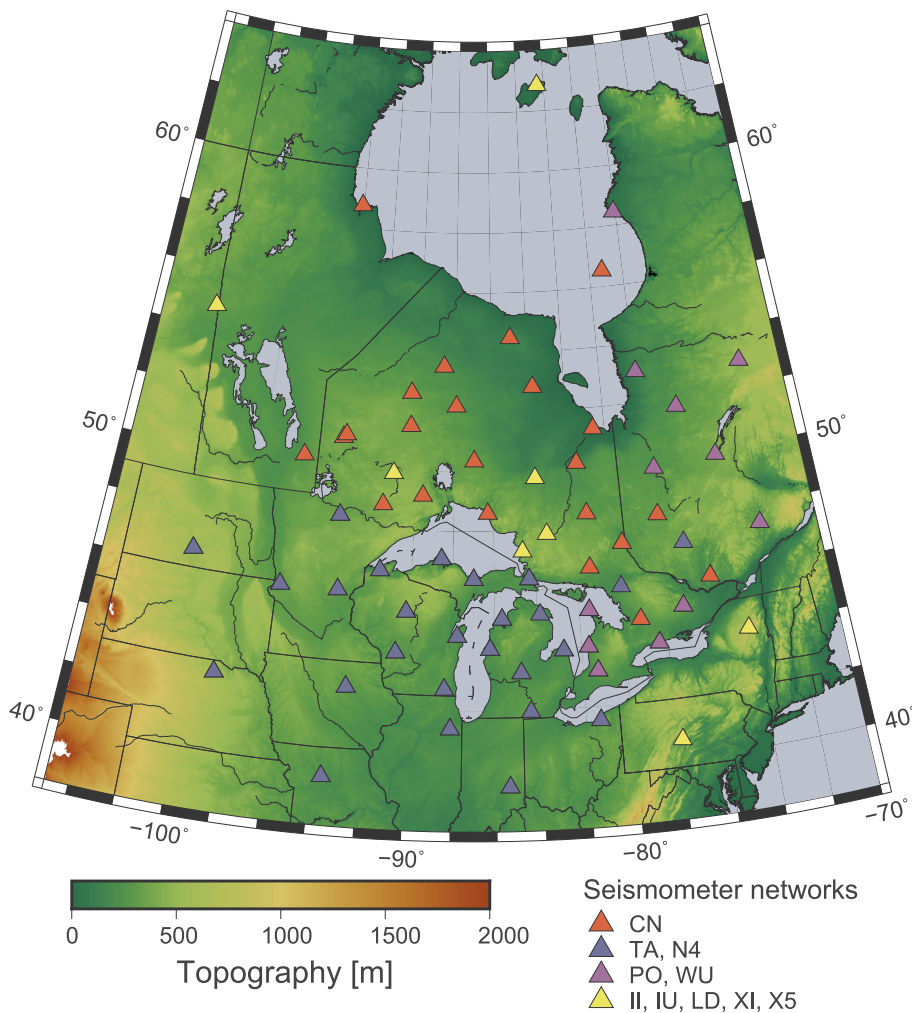


Fig. 2. Location of all stations used in this study. Network codes: CN, Canadian National Seismograph Network; TA, USArray Transportable Array; N4, Central and Eastern US Network (CEUSN); PO, Portable Observatories for Lithospheric Analysis and Research Investigating Seismicity (POLARIS); WU, Southern Ontario Seismic Network; II, IRIS/IDA Seismic Network; IU, Global Seismograph Network (GSN); LD, Lamont-Doherty Cooperative Seismographic Network; XI, Superior Province Rifting Earthscope Experiment (SPREE, 2011–2013); X5, Hudson Bay Lithospheric Experiment (HUBLE, 2007–2011). See [Supplementary material](#) for full network references.

low smoothing values of 0.1 (isotropic) and 0.2 (anisotropic). Finally, additional tests were run to select the preferred balance between the two parameters. Further details are given in the [Supplementary material](#).

Final parameter selection was made after examining model results at all periods to be used for inversion, for a range of parameters near the best approximate smoothing and damping values ([Table 1](#)). We vary the parameter choice with period, to help compensate for the differing path coverage and resolution due to wavelength variations. The following observations contributed to the final choice: first, damping (equivalent to penalizing the difference between neighboring nodes, or first derivative) more strongly diminishes anisotropy patterns in comparison to smoothing (equivalent to penalizing difference between a point and nearby average, or second derivative). Because of this, we keep damping fairly low for anisotropy. Additionally, variance reduction seems to be slightly better for higher smoothing/lower damping combinations of parameters. Thus, the smoothing parameters are typically 3–5 times larger than the damping parameters. Second, increasing the damping for one parameter (e.g., for anisotropy but not for isotropy) dramatically pushes heterogeneity into the lower damped parameter (e.g., isotropy), much more noticeably than increasing the smoothing for a single parameter does. So, anisotropic damping parameters are quite close to isotropic damping parameters. Lastly, it is generally expected that anisotropy will be less well constrained than isotropic velocity, so anisotropic smoothing and damping parameters should always be higher than isotropic parameters.

4. Resolution tests

Resolution tests were conducted at several periods, representing short (20–40 s), medium (45–120 s), and long periods (140–220 s), as well as a variety of path coverage levels (low, 180 s; medium, 30 s; high, 60 s). All tests are conducted with the same framework: creating a synthetic phase velocity model, calculating synthetic measurements from that model, adding in 0.02 km/s random noise, and then inverting the measurements for an output anisotropic phase velocity model, using the same path coverage and inversion parameterization as was applied to the real data.

In this section, we describe the results of two types of resolution test, one using geometric shapes (the equivalent of the standard checkerboard test used in most tomographic studies) and the other using a synthetic model based on surface tectonic boundaries. Descriptions of further tests of isotropic and anisotropic resolution (linear gradients, isotropic-anisotropic leakage and rotated anisotropy) are described in detail in the [Supplementary material](#).

4.1. Checkerboard tests

Checkerboard tests are typically used to show how well individual small anomalies, and sharp contrasts in velocity over short distances, can be resolved by the methods used. They are mainly influenced by the path coverage and smoothing and damping parameters selected, and do not encompass all the uncertainty in the resulting maps. The following variations on checkerboard tests were carried out for isotropic phase velocity at 30, 60, and 180 s period ([Fig. 4](#)):

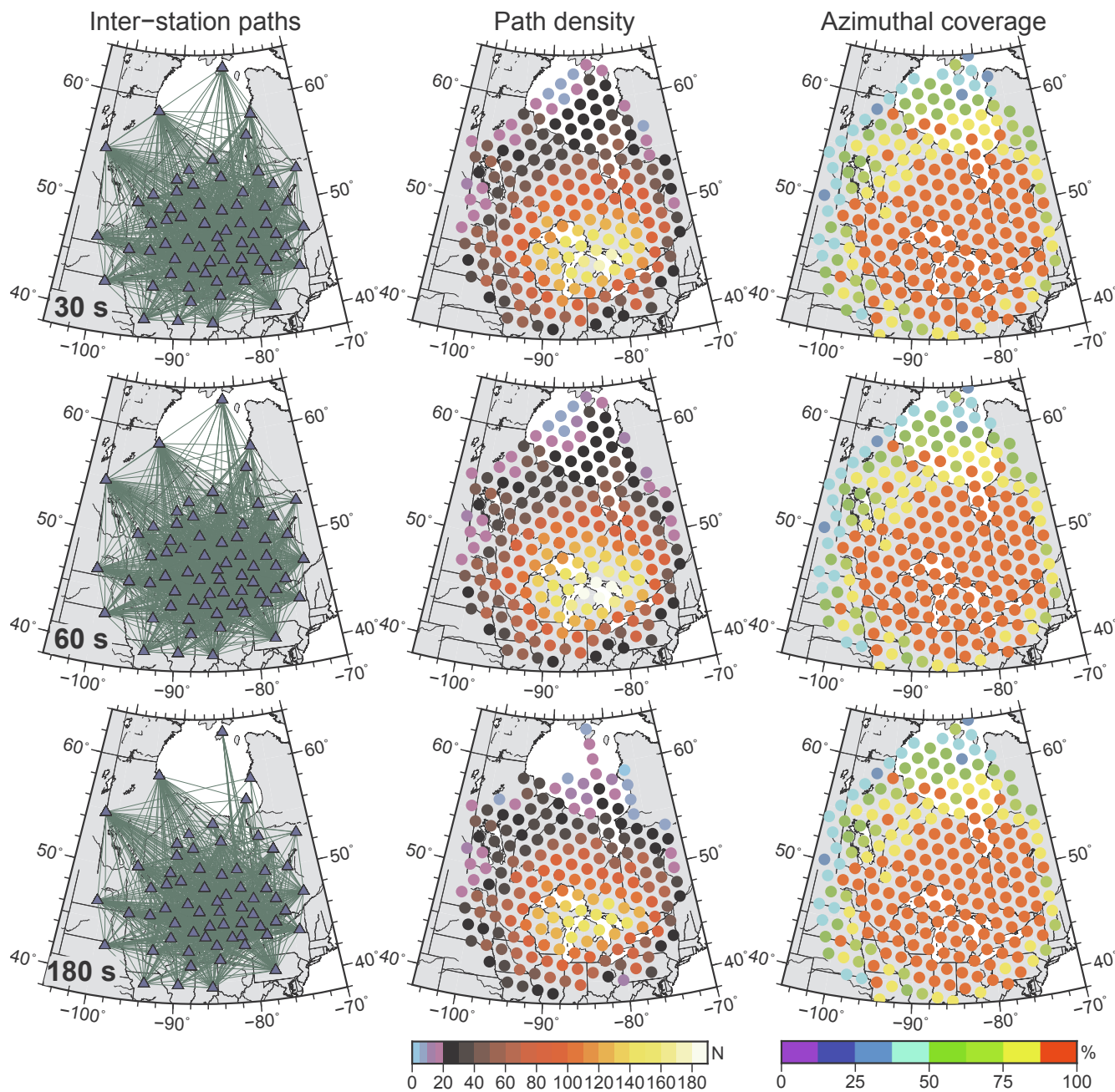


Fig. 3. Station path coverage (left column), number of paths crossing each grid node of the phase velocity map inversion (center column), and percent of azimuthal bins with path coverage at each grid node (right column), for 30, 60, and 180 s period. Azimuthal bins are 22.5° wide and consider 180° of path orientations.

Table 1
Final inversion parameters.

Period (s)	Smoothing parameters		Damping parameters	
	Isotropic	Anisotropic (2ψ and 4ψ)	Isotropic	Anisotropic (2ψ and 4ψ)
20–35	0.35	0.55	0.05	0.10
40–140	0.75	0.95	0.20	0.25
150–160	1.10	1.25	0.35	0.35
175–220	1.20	1.30	0.40	0.40

1. 450 by 260-km hexagons: At 30 and 60 s period, anomalies are clearly recovered throughout the study area; only the northwestern anomaly in Manitoba is significantly reduced in amplitude. At 180 s, the northern two anomalies and the southeastern edge anomaly are

not recovered. The shape and amplitude of the phase velocity anomalies in the central study area are reproduced well. Weak spurious anisotropy is observed in the north (Hudson Bay) at 60 and 180 s periods.

- 150-km triangles: These small anomalies, approximately the size of the station spacing, are recovered very well throughout the Great Lakes region at 30 s period, and the low-velocity anomalies are still observable at 60 s period. At 180 s period, the locations of the anomalies are still detectable, but the amplitude of anomalies is quite small.
- 260-km-wide stripes, oriented NNW-SSE: The stripes are well-recovered at all periods in terms of location, orientation, and amplitude of anomalies, south of 56°N latitude (30 s), 54°N (60 s), and 52°N (180 s).

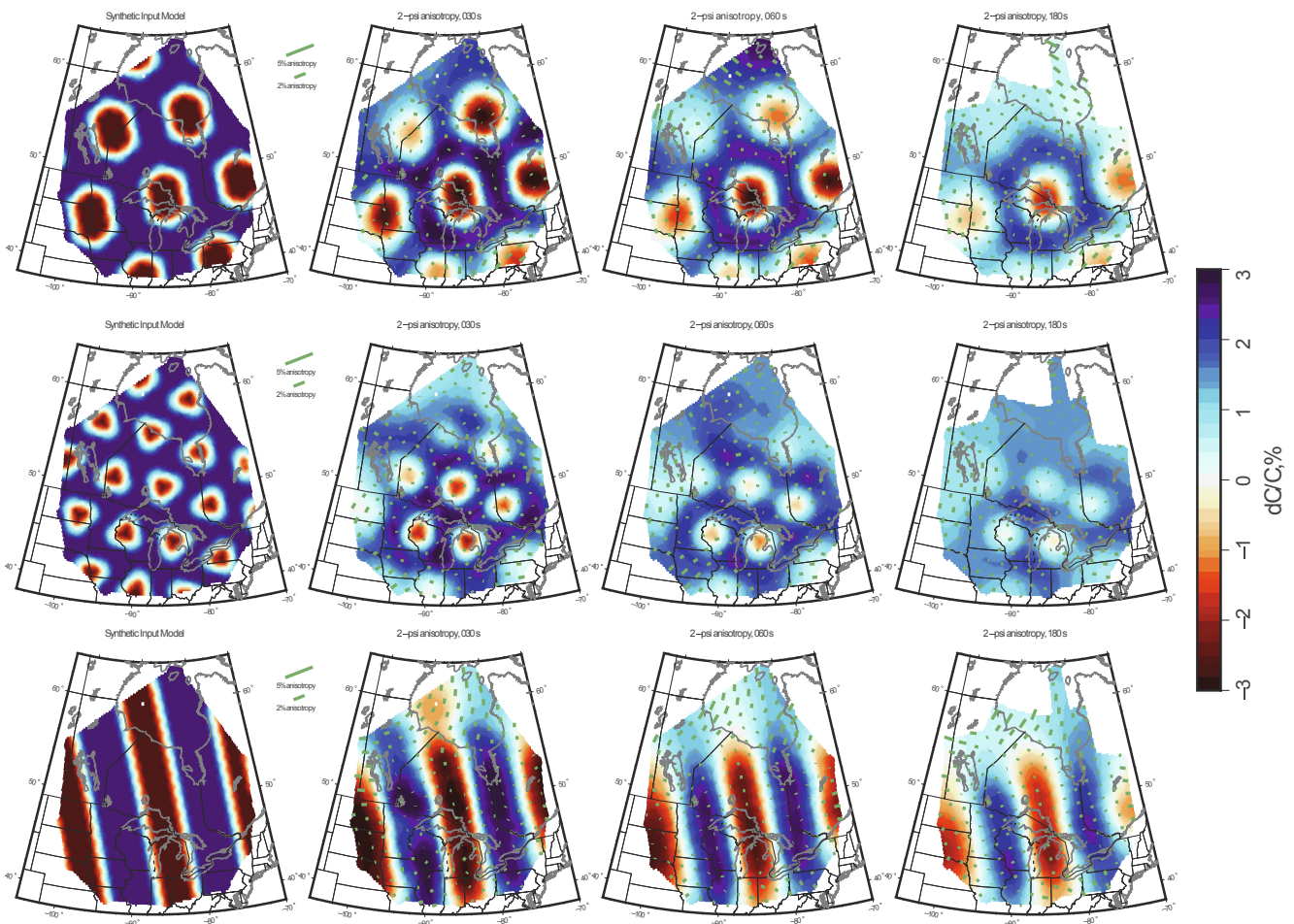


Fig. 4. Checkerboard tests for 30, 60, and 180 s periods. Synthetic input models are created by setting grid nodes to a positive or negative phase velocity anomaly (left column), and are then used to calculate synthetic measurements and invert for a new model, with the same path coverage and inversion parameters as the real data.

4.2. Resolution tests for tectonic features

Based on the map of basement terranes from [Whitmeyer and Karlstrom \(2007\)](#) (Fig. 1), we create synthetic input models for major tectonic features of our study region. Bearing in mind that the velocities in the synthetic input model are an extreme case of fast or slow anomalies with sharp boundaries, we examine the output models to see if the data coverage and inversion could resolve such features (Fig. 5).

1. Superior Craton: We create an isotropic input model consisting of a fast anomaly following the boundaries of the Superior craton, surrounded by slow velocities representing the Proterozoic orogenic belts. At 30 s period, the anomaly is well recovered in the output model, with accurate boundaries except for some smearing in the northwest corner. Spurious anisotropy is minimal, only appearing along the western boundary of the province, near the edge of the study area where velocity gradients are sharp.
2. Trans-Hudson Orogen (THO): Previous studies of the Hudson Bay region ([Pawlak et al., 2012](#); [Darbyshire et al., 2013](#)) indicate a low-velocity anomaly in the shallow lithosphere of southern Hudson Bay, and a near-vertical relatively low-velocity feature coincident with the surface signature of the Trans-Hudson orogen. We create a synthetic input model with an isotropically slow velocity anomaly following the boundaries of this terrane, surrounded by fast velocities. This terrane largely follows the edge of the study area, and is in the region of the study area with the poorest path coverage. Despite this, the output velocity model at 30 s period shows weakly

slow isotropic anomalies following the shape of the terrane, with a high-amplitude slow anomaly beneath the southern part of Hudson Bay. As with the previous test, the only spurious anisotropy resulting from this input model occurs along the western edge of the study region, near the sharp velocity gradient.

3. The Mid-Continent Rift (MCR): A key question in this study is whether the Mid-Continent Rift, which is visible as a prominent set of anomalies in potential-field maps, has a continuous signature in the crust and mantle lithosphere. We examine the expected resolution of this study for a synthetic isotropic input model of slow velocities following the MCR, surrounded by fast velocities, at 30, 60, and 180 s period. This is a narrow anomaly, which can be difficult to observe using surface waves; however, at all periods the shape of the anomaly is recovered. At 30 and 60 s period, the strongest slow anomaly beneath Lake Superior is also fairly well recovered. At longer periods, the amplitude of the anomaly is greatly decreased, coherent with the change of path coverage. We do not necessarily expect the long-period phase velocity maps to reflect the crustal geology; the tests at 60 and 180 s period are instead a check to see how the differing path coverage and longer wavelengths affect the signal.

5. Phase velocity maps

Our phase velocity maps are shown for selected periods between 20 and 220 s in [Figs. 6 and 7](#), with the complete set shown in the [Supplementary material](#). As discussed in Section 2, we invert for

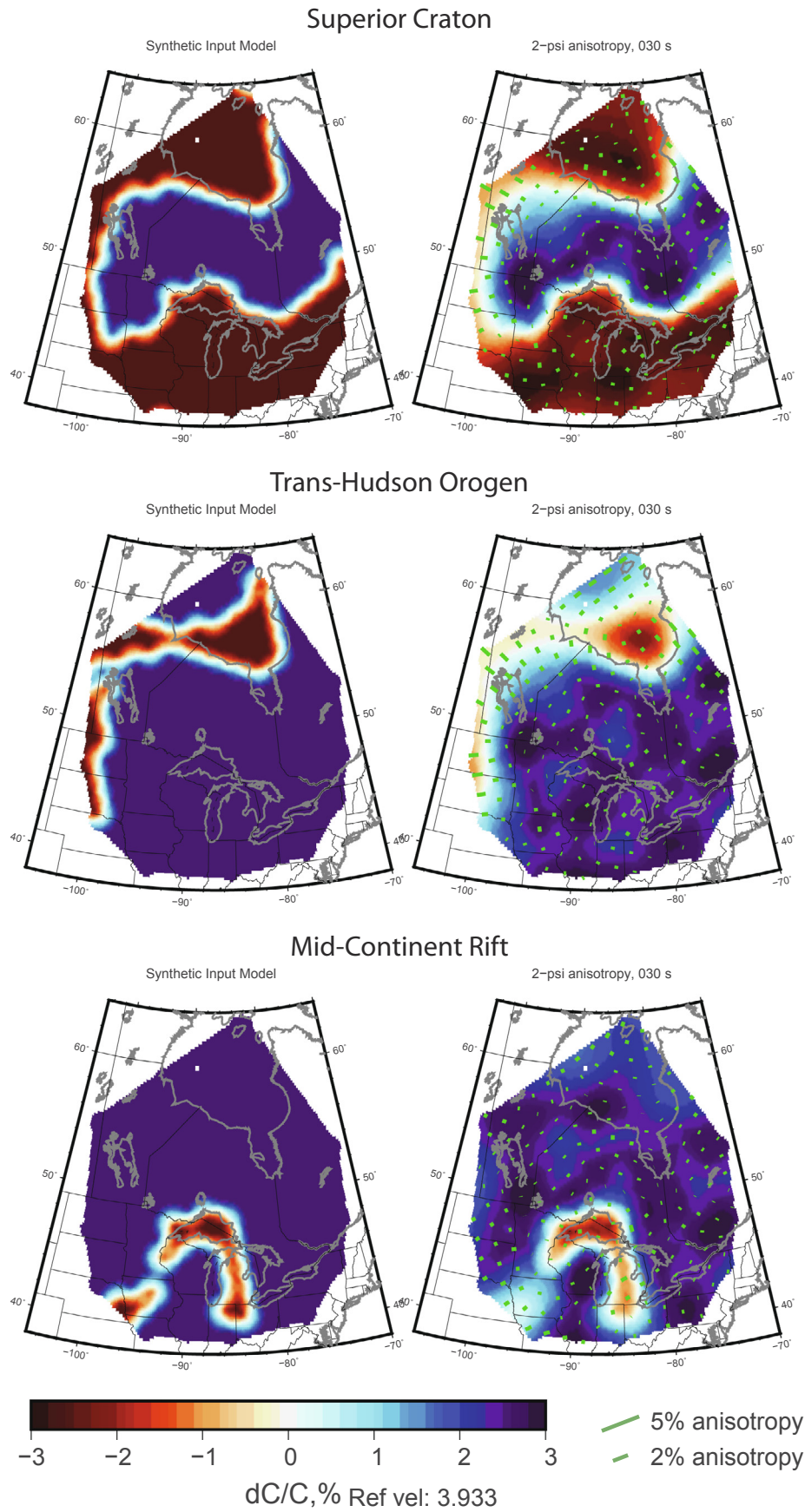


Fig. 5. Left column: synthetic input models created using three tectonic provinces from [Whitney and Karlstrom \(2007\)](#) (see [Fig. 1](#)). These models were used to calculate synthetic measurements for 30 s period, which were inverted for phase velocity maps using the same path coverage and inversion parameters as for the real data. Right column: Resulting phase velocity maps.

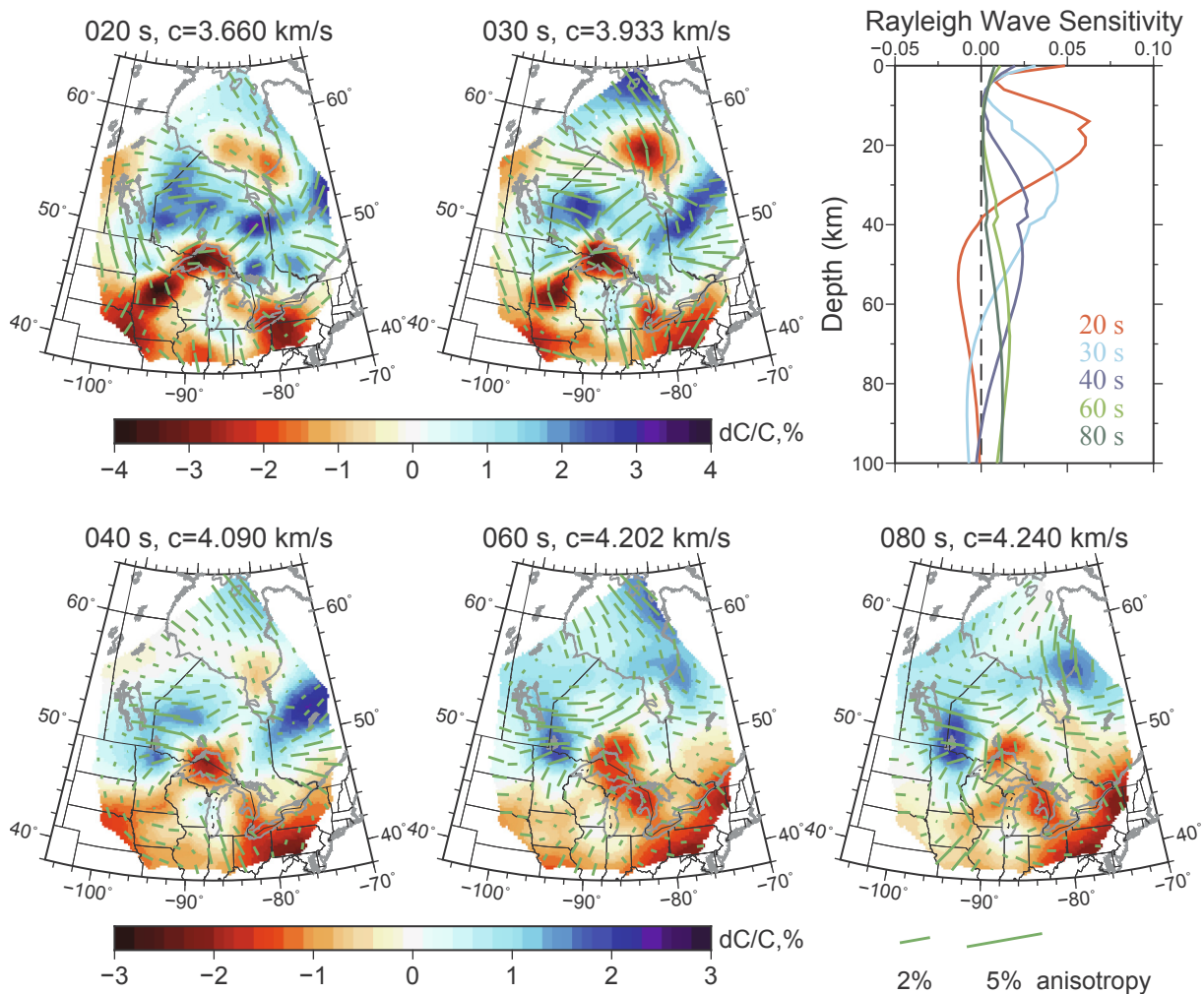


Fig. 6. Final Rayleigh wave phase velocity maps at selected periods, 20–80 s. Isotropic phase velocity for each subplot is shown as a percent deviation from the regional average at that period (c). Green bars show direction and magnitude of anisotropy. Top right subplot shows Rayleigh wave sensitivity to V_s structure with depth for each period, calculated using the AK135 1-D model (Kennett et al., 1995), modified for a 40 km thick crust, to aid in interpretation. (For interpretation of the references to colour in this figure legend, the reader is referred to the web version of this article.)

isotropic, 2ψ , and 4ψ anisotropic heterogeneity; however, we do not interpret 4ψ anisotropy, which is not well constrained by the data and is typically small. As phase velocity predominantly represents an integrated shear velocity over a range of depths, we include sensitivity kernels for the periods shown to aid the reader in interpreting the figures.

At short periods, 20–30 s, Rayleigh waves are predominantly sensitive to the shear velocity structure at depths of around 20–70 km, as shown in Fig. 6. With respect to the regional average velocity at each period, we observe isotropic anomalies of up to $\pm 4\%$, with the most striking feature being an arcuate slow anomaly running from south-eastern Minnesota, up to Lake Superior, and down to western Pennsylvania. The majority of Ontario and western Quebec overlie significantly fast velocities, spatially correlated with the Archean Superior craton, and another slow anomaly is present in southern Hudson Bay. The anisotropic signals are very heterogeneous, with nearly all values less than 2%.

At moderate periods, 40–60 s, the depth of principal sensitivity to shear velocity structure ranges from ~ 40 to 130 km. Isotropic velocity anomalies at these periods range up to $\pm 2.3\%$ from the regional averages, and structure is noticeably smoother than at short periods. We observe relatively lower velocities in the Great Lakes region and to the south, and higher velocities throughout eastern Manitoba, Ontario, and northwestern Quebec. Anisotropic fast orientations are mostly E–W

or NE–SW trending north of the Great Lakes, with very weak anisotropy beneath the Great Lakes and to the south.

At longer periods, 100–220 s, sensitivity to shear velocity structure is strongest at depths of 80–400 km. Isotropic velocity anomalies reach up to $\pm 2.7\%$ from the regional averages, but most values are less than 1%. Slow isotropic phase velocity anomalies are still present in the Great Lakes region, but also throughout nearly the entire eastern half of the study area. The western half of the study area shows generally faster velocities, with the fastest velocity in northwestern Ontario. Anisotropy values become progressively larger with increasing period, reaching values of up to 3.5% at 220 s period, with fast orientations trending mainly E–W in Quebec and eastern Ontario, and NE–SW in the western half of the study area.

At periods corresponding to crustal/uppermost-mantle depths, we observe a distinct contrast between the relatively high velocities beneath the Superior craton and the lower velocities beneath the Trans-Hudson Orogen and Mid-continent Rift (MCR). Our “structural” resolution tests (Section 4.2) indicate that these variations in phase velocity are robust features, despite some of them being located at the edge of our study region. At 30 s period, the arcuate shape of the anomaly beneath the MCR is shown to be a resolvable feature by our structural tests. We note that the location of the eastern branch of the MCR-related low-velocity anomaly is approximately 100 km farther to the east in the results from data than the MCR as mapped by potential

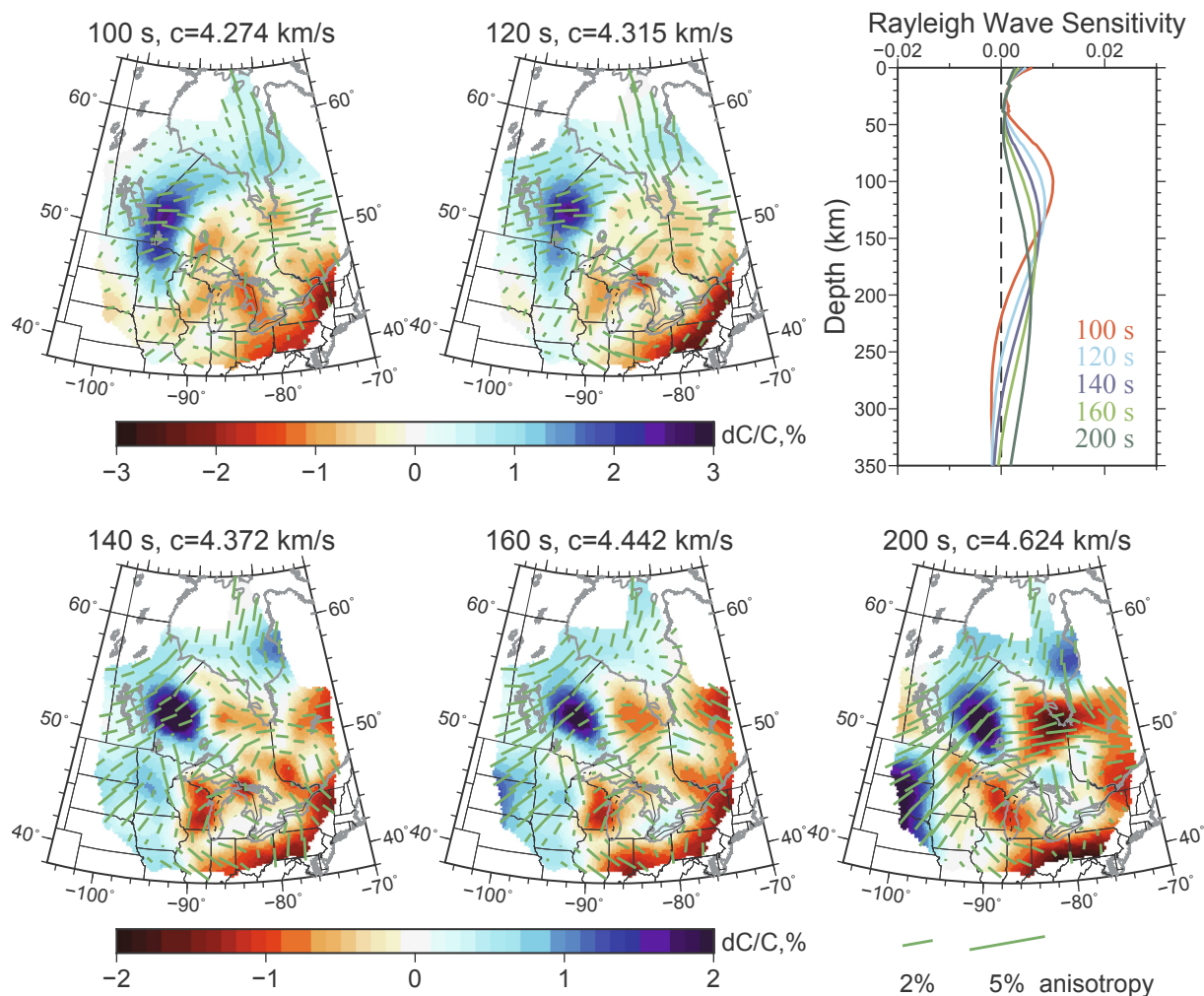


Fig. 7. Final Rayleigh wave phase velocity maps at selected periods, 100–200 s. Plotting conventions as for Fig. 6.

field data. At 60 s period, the anomaly under Lake Superior is broader, extending farther to the north than the near-surface location of the MCR and, again, the eastern branch of the anomaly is shifted to the east with respect to the MCR's near-surface footprint. At 180 s period, the slowest anomaly is no longer directly under Lake Superior, but instead located just west of Lake Michigan.

6. Discussion

6.1. Phase velocity variations and lithospheric structure

Variations in phase velocity can result from a variety of physical causes, including differing temperature, composition, and volatile content. As such, interpretation of phase velocity is best carried out in conjunction with other information, including geologic context, geochemical information, or other geophysical measurements. Here we discuss our observations of phase velocity in several sub-regions with these factors in mind.

6.1.1. Superior Craton

The Superior Craton is well known to exhibit fast seismic velocities (e.g., Frederiksen et al., 2013; Bollmann et al., 2019; Boyce et al., 2019; Darbyshire and Lebedev, 2009; Petrescu et al., 2017; Schaeffer and Lebedev, 2014), and our observations are consistent with these previous findings. Based on our resolution tests at 30 s period, even if the Superior craton was seismically homogeneous, we would observe apparent velocity variations in the far northwest (Manitoba) and south

(Nipigon Embayment) of the craton due to path coverage and velocity gradients at the craton edges. However, our tests show that phase velocity variations observed within all other parts of the craton are most likely due to real tectonic features.

Our 30 s phase-velocity map shows high velocities stretching across northwestern Quebec and in western Ontario, but with a noticeable disconnect between the two in central-eastern Ontario. This indicates some real variability within the Superior Craton at lower-crustal depths. The source of this variability could be compositional (including associated variations in crustal heat production) (e.g., Mareschal and Jaupart, 2004; Percival et al., 2006), crustal thickness variations (e.g., Hammer et al., 2010; Darbyshire et al., 2007; Petrescu et al., 2016; Zhang et al., 2016), and/or later modification of crustal material (e.g., Heaman and Moser, 1997).

Up to 50 s period, even considering internal variations, all of the Superior has fast velocities relative to the surrounding regions. However, at 100 s period and longer, only the western half of the Superior craton continues to show exceptionally high velocities (Fig. 8). The eastern half of the Superior has velocities similar to those of the adjacent Proterozoic orogens. This is consistent with previous body-wave studies that have observed this division at mantle depths (e.g., Frederiksen et al., 2013; Bollmann et al., 2019). The east–west variation is clearly related to differences in the lithospheric root; cratonic roots are typically fast because they are cold and depleted, but they can be metasomatized to varying degrees (e.g., Jordan, 1988; King, 2005). The lower velocities beneath the eastern Superior have been suggested to be due to lithospheric refertilization from passage of the Great Meteor

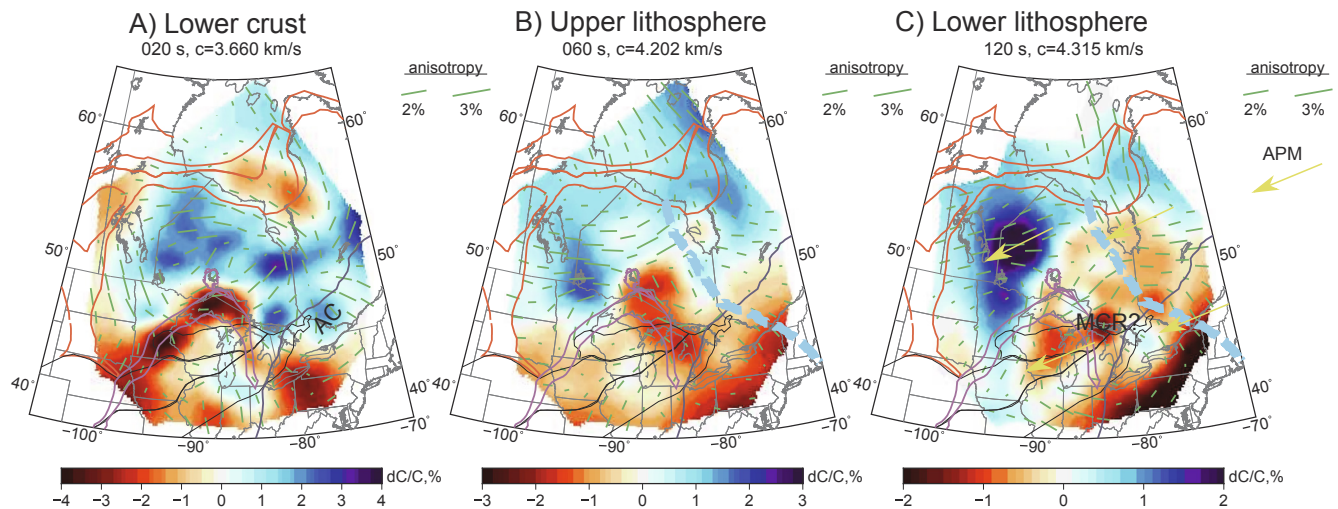


Fig. 8. Representative phase velocity maps for (a) lower crust, (b) upper to mid-lithosphere, (c) lower lithosphere/ sublithosphere, with interpreted features marked. AC = Archean crust; MCR = Mid-Continent Rift; WS = Western Superior lithospheric root. Boundaries of the Trans-Hudson orogen (red), MCR (purple), Grenville Front (blue), GM hotspot track (light blue), and Penokean/Yavapai/Mazatzal orogens (black) are overlain (Superior craton is delimited by red, purple, and blue). Approximate absolute plate motion taken from HS3-NUVEL 1A (Gripp and Gordon, 2002). (For interpretation of the references to colour in this figure legend, the reader is referred to the web version of this article.)

hotspot (Frederiksen et al., 2013), or variations in lithospheric thickness (Petrescu et al., 2017).

MT studies show considerable lateral variability in the lithospheric structure of the Superior. In southeastern Ontario, the Archean Superior lithosphere is resistive to depths of ~150–280 km, but has a conductive lower lithospheric layer that the authors interpret to have been metasomatized during the Cretaceous passage of the Great Meteor Hotspot, adding water but not substantially altering the density or thermal structure of the region (Adetunji et al., 2015). The conductive lower lithosphere correlates with relatively low phase velocities in our model, suggesting that these velocity anomalies are the seismic signature of lower-lithosphere metasomatism.

6.1.2. Proterozoic orogens

As discussed above, the Trans-Hudson Orogen (THO) marks the beginning of the assembly of the North American continent, and consists of a series of accreted arcs and oceanic terranes brought together by subduction processes. These terranes have since been modified and stabilized by processes including crustal thickening and imbrication, granitic intrusions, and lithospheric differentiation (Bowring and Karlstrom, 1990; Keller et al., 2005; Whitmeyer and Karlstrom, 2007). The lithosphere beneath these accreted terranes is thought to be thick and buoyant, but not as strong as that beneath the Superior Craton due to compositional differences (Whitmeyer and Karlstrom, 2007). These same types of materials and processes were later involved in the Yavapai, Mazatzal, Granite-Rhyolite, and Grenville orogens surrounding the Superior Craton.

The phase velocities in the vicinity of the Trans-Hudson Orogen (THO) are slow relative to the extremely fast velocities in the Superior Craton. This distinction is most apparent at 20–40 s period, implying that the velocities largely reflect a crustal signature (Fig. 8). However, the THO is found on the edge of our region of coverage and, particularly at longer periods, may be less well constrained than the center of the study region. At longer periods and greater depths, our study is inconclusive as to whether there are significant differences in velocity between this area and the sub-Superior Craton; however, we note that previous studies that have also covered this area do observe differences between the mantle lithosphere in the two regions (Darbyshire et al., 2013).

Within the crust of the THO where measurements are available, heat flow is highly variable, just as it is in the Superior craton (e.g.,

Mareschal et al., 2005; Perry et al., 2010; Jaupart et al., 2014). In addition, the amalgamated shield resulting from the THO collision has been tectonically stable for at least the last ~1.70–1.65 Ga (Schneider et al., 2007; Hammer et al., 2010). Thus, the large-scale difference between these two regions can likely be attributed to compositional differences in crustal material, rather than thermal variations. Measurements of crustal thickness are highly variable throughout: in the vicinity of Hudson Bay, where thicknesses vary from 40 to 50 km (Gilligan et al., 2016); west of the Superior craton, thicknesses vary from 37 to 52 km over length scales as short as 50 km (Zelt and Ellis, 1999). In some areas, the original pre-collision Moho is preserved, while in others, the Moho formed during post-collisional processes like gravitational collapse or lower crustal delamination (White et al., 2000). The topography of the Moho may contribute to the small variations in phase velocity within the THO, however, we note that the strongest slow anomaly, found beneath Hudson Bay (an area of thicker crust), coincides with the slowest anomaly based on path coverage and geometry of the THO in our resolution test.

The phase velocities beneath the younger Proterozoic orogens (Yavapai, Mazatzal, Granite-Rhyolite, and Grenville) are all slower than those beneath the Superior Craton, particularly at 20–60 s period. However, they are not as distinctly slow as the THO. Based on the depths influencing these measurements, part of this difference is likely due to crustal thickness. The Superior Craton has been shown to have a relatively thin (32–42 km) crust with a very flat Moho (Musacchio et al., 2004), as is typical of Archean crust. The Grenville and other provinces have consistently thicker crust (~42–52 km, Ludden and Hynes, 2000; Shen and Ritzwoller, 2016), thus juxtaposing slower crustal material in Proterozoic regions next to faster mantle material in the Superior craton at the same depth. At 100–220 s period, these regions exhibit similar velocities to the eastern Superior, but none have the extremely high velocities observed in the western Superior. This may be attributed to the differing plate tectonic conditions that existed in Archean versus Proterozoic times, and likely resulted in different melt, pressure, and temperature conditions for the formation of cratonic lithosphere (e.g., Korenaga, 2006). Extensive metasomatism due to long-lived Andean-style subduction may have decreased P-wave velocities in the Grenville lithosphere (Boyce et al., 2019), but this could have a smaller effect on S-wave velocities and consequently, on Rayleigh wave velocities (Wagner et al., 2008; Schutt and Lesher, 2010). Lithospheric thicknesses are greater than 175 km throughout the whole

study area (Priestley et al., 2019), and should not contribute greatly to the phase-velocity variations.

6.1.3. Mid-Continent Rift (MCR)

Given the huge amounts of magmatism produced by the 1.1 Ga MCR, it is no surprise that there is a strong phase velocity anomaly at shorter periods. Composed of dominantly basaltic material, one might expect a fast phase-velocity anomaly; however, what is observed in our short-period (20–40 s) results is a strong low-velocity anomaly, in a clear arcuate pattern that approximates the rift location as outlined by other types of data, such as gravity and magnetic anomaly patterns (Fig. 8). The strongest anomalies are beneath Lake Superior and the western branch of the MCR. This can be explained as a combination of thick crust due to mafic underplating, and the presence of thick sediments. Receiver function analysis suggests the crustal thickness within the western branch of the MCR may be greater by 10–15 km or more than surrounding regions (Zhang et al., 2016), and this material is likely slower than the adjacent lithospheric mantle. Additionally, the rift basins created by the MCR subsided significantly due to the weight of the mafic underplating as well as the extension, and filled with low-velocity sediments following the emplacement of ~20 km thickness of volcanics. These sediments reach ~5–8 km thickness (Green et al., 1989), and can contribute significantly to a low-velocity surface wave signal at short periods.

At longer periods, the western branch of the MCR appears as a moderately low-velocity anomaly, while Lake Superior and the eastern branch of the MCR overly lower velocities. At 60–100 s period, the Lake Superior low velocity anomaly shifts to the north. This coincides with the Nipigon Embayment, another region of basaltic magmatism related to the early activity of the MCR (Hart and MacDonald, 2007). A low-velocity anomaly in this area has been noted in body-wave tomography (Frederiksen et al., 2007; Frederiksen et al., 2013). However, due to the lack of stations within Lake Superior, those studies posed questions about the connection of this anomaly to the rest of the MCR. In our phase-velocity results, the mantle anomaly beneath the Nipigon Embayment appears to be smoothly connected to shallower velocity anomalies beneath Lake Superior that are part of the main MCR axis. However, this does not preclude the involvement of a plume, by modifying the lithosphere and crust prior to the MCR (Hollings et al., 2004) or by initiating MCR rifting (Heaman et al., 2004). A 3D shear velocity inversion based on these phase-velocity maps could more clearly demonstrate the depths and continuity of these velocity anomalies.

Finally, a key question in this area is whether the mantle beneath the main axis of the MCR, south of the Nipigon Embayment, bears the signature of lithospheric modification, or whether the slow crustal velocities and thickened crust are sufficient to cause the moderately slow Rayleigh wave anomalies we observe at long periods. The shift in the strongest low-velocity anomaly towards the east with increasing period indicates that if there is lithospheric modification, it may be tilted (Fig. 8)). 3-D shear-velocity inversions using only TA data favor low velocities related to the rift at shallow depths only (Pollitz and Mooney, 2016). Including the Canadian data from this study in a 3-D shear velocity inversion may provide the tools to address this further.

6.1.4. Great Meteor (GM) hotspot track

A low-velocity mantle corridor is observed in the inversion of P-wave travel time delays; the feature is 120 km or less in width, strikes NW-SE, and is located at 100–300 km depth (Rondenay et al., 2000; Boyce et al., 2016). Two main processes were proposed: a fixed mantle plume, or continental rifting. If it is in fact related to a mantle plume, the low-velocity lineament is generally considered to be the track of the Great Meteor hotspot, which may have exploited lithospheric weaknesses related to previous rifting events (e.g., Boyce et al., 2016). In the body wave studies, the low-velocity anomaly is too narrow to be solely explained by a present-day thermal perturbation (Eaton and

Frederiksen, 2007); additional contributions may come from compositional anomalies such as iron-rich rock related to decompression melting and/or some effects from changes in anisotropy (Rondenay et al., 2000). In our long-period results, we observe low velocities in the same area as the low-velocity mantle corridor from the Rondenay study, at approximately 78°W and 46°N. Additionally, at 140 s period, the anomaly takes on a linear shape with a NW-SE orientation, although it is much broader in the surface wave results, as one might expect.

Although the GM hotspot was the most recent modification of the lithosphere in this region, dating of diamonds from the Attawapiskat region shows an age of formation of ~720 Ma, after the diamond-deforming heat from the nearby MCR dissipated and during rifting to the north during break-up of Rodinia (Smit et al., 2014; Aulbach et al., 2018). This indicates that the lower mantle may have been refertilized and metasomatized even before the passage of the Great Meteor hotspot, which later provided the pathway to the surface for the diamonds. Thus, the region experienced three potential refertilization events after cratonization: MCR, Rodinia breakup/Franklin LIPs, and the GM hotspot.

6.2. Seismic anisotropy and the subcontinental mantle

As noted by Schaeffer et al. (2016), global isotropic velocity models from the community are near consensus. However, azimuthal anisotropy models have not yet reached that stage. Thus, particularly where dense seismic data are available, regional models to constrain anisotropy are valuable. Variations in anisotropy with depth have been observed for many years (e.g., Vinnik et al., 1989) and can reflect variations in crustal layering (e.g., Dalton and Gaherty, 2013), mid-lithospheric discontinuities (e.g., Rychert and Shearer, 2009), as well as the base of the lithosphere and adjacent asthenospheric flow directions (e.g., Nishimura and Forsyth, 1989; Plomerová et al., 2002; Schaeffer et al., 2016). Surface wave studies provide constraints on these variations in depth, and can be used in combination with other methods like SKS splitting.

6.2.1. Potential sources of seismic anisotropy

Our phase velocity maps sample a range of depths extending from the lower crust to the sublithospheric mantle. We must therefore consider a number of potential sources for seismic anisotropy depending on the period. In the lower crust, the foliation and lineation of metamorphic rocks in response to past deformation is the most likely source, as it leads to the alignment of anisotropic minerals such as amphiboles and micas (e.g. Brocher and Christensen, 1990; Meltzer and Christensen, 2001). Depending on the complexity of the crustal deformation, such alignments may have a predominantly 2ψ symmetry, or include a 4ψ component. In the lithospheric mantle, deformation may cause lattice-preferred orientation (LPO) of olivine, where the a -axes align with the deformation direction to form a distinct anisotropic fabric for which Rayleigh waves detect a 2ψ symmetry (e.g., Silver and Chan, 1988; Silver and Chan, 1991; Vauchez and Nicolas, 1991; Bastow et al., 2007; Karato et al., 2008). Beneath the lithosphere, present-day mantle flow also causes strain that aligns olivine a -axes with the flow direction, resulting in an LPO-related anisotropic fabric (e.g., Zhang and Karato, 1995; Bystricky et al., 2000; Tommasi et al., 2000). Given that the most recent significant magmatic episode beneath any part of our study region occurred over 100 Ma ago, we do not consider fluids/melts to contribute to the anisotropy that we find.

6.2.2. Crustal anisotropy

Azimuthal anisotropy at short periods (20–35 s), related to crustal signatures, is highly variable. We observe dominantly E–W fast orientations in the western Superior, NE–SW fast orientations in the central Superior, and E–W fast orientations in the eastern Superior. These variations are likely due to the tectonic stresses at the time of accretion of the various terranes that make up the Superior craton,

which resulted in layering, fracturing, and the alignment of anisotropic minerals. There is a distinct change in fast orientation within the Mid-Continent Rift and to the south, with smaller amplitudes and more heterogeneity. Lateral smoothing due to the nature of surface waves makes more specific interpretation of shallow anisotropy difficult; we focus on the subcontinental mantle for the remainder of the discussion.

6.2.3. Archean and Proterozoic lithosphere

At periods sensitive to lithospheric depths (40–120 s), we observe the strongest anisotropy in the Superior craton, particularly beneath the western Superior. This is consistent with global observations showing greater anisotropy in Archean provinces than in other continental regions via shear wave splitting (e.g., Vinnik et al., 1995; James and Assumpcao, 1996; Ferré et al., 2014). The origin of the E–W fast orientations may be very old; it has been suggested that parts of continental lithosphere, if they were formed by the stacking of subducted oceanic lithosphere, may maintain the frozen anisotropy from the original oceanic plates (Babuška and Plomerová, 1989; Babuška and Plomerová, 2006). This orientation parallels the terrane boundaries within the western Superior (Fig. 1). The terrane boundaries are more complex in the central-eastern Superior, which could explain the variations in fast orientation and weaker anisotropy observed in this region.

A similar variation in seismic anisotropy between the western and central-eastern Superior has been observed in shear wave splitting studies (Fig. 9; e.g., Frederiksen et al., 2013; Ola et al., 2016), where the western Superior is characterised by extremely strong splitting. The spatial variability of the splitting parameters was used to interpret a dominantly lithospheric contribution to the observed seismic anisotropy, and this is consistent with the period range at which we observe the strongest phase-velocity anisotropy.

The small values of anisotropy observed beneath Proterozoic orogens could be indicative of any of the following: variable azimuthal anisotropy over short vertical or horizontal distances that averages to null, a vertical fast orientation, or destruction/modification of the original frozen anisotropy in the lithosphere. The highly heterogeneous fast orientation hypothesis is supported by previous studies in the North American craton (Gaherty, 2004). A vertical fast orientation is

compatible with the observations, but more difficult to explain tectonically. The last hypothesis, modification of the anisotropy in the lithosphere, will be discussed in the following section.

6.2.4. Effects of lithospheric modification: the MCR and the GM

Mantle plumes produce melt in the lithosphere, which can erase anisotropy, but for the most part, melt appears to be confined to small areas. The main effect of a plume is to enrich mantle olivine with iron, reducing the Mg# as well as reducing seismic velocities; however, it does not alter seismic anisotropy unless the lithosphere is destroyed (Tommasi et al., 2004). This is consistent with our observations of phase velocity and azimuthal anisotropy in the region that has been affected by the Great Meteor hotspot: Rayleigh wave phase velocity is lower in the eastern Superior by approximately 2% compared to the western Superior at 60–120 s period, but anisotropy generally follows the directions of the terrane boundaries in both parts of the craton. This may represent what Vauchez et al. (2005) call transitional lithosphere.

It is likely that the lithosphere in our study area also interacted with a plume during the formation of the Mid-Continent Rift (Stein et al., 2015; Stein et al., 2018). We therefore expect the mantle lithosphere to have lower velocities than surrounding areas. However, in phase velocity maps it is not possible to differentiate this low velocity signature from the strong low velocity signature generated by the shallow structure of the rift. Anisotropically, it appears that the large volumes of melt generated in this region may have been enough to disrupt the alignment of olivine in the lithosphere. If the accretion of terranes in large orogenic events was the main determinant in fast orientation previously, we would expect E–W or NE–SW fast axes south of Lake Superior. Instead, we observe very weak anisotropy, with some coherent fast orientations paralleling the eastern branch of the MCR at 40–60 s period. At 80–120 s period, the anisotropy is still weak, and highly heterogeneous. Shear wave splitting measurements (the cumulative delay time due to azimuthal anisotropy throughout the entire mantle) in this region are highly uniform in fast orientation, parallel to absolute plate motion (Fig. 9; Ola et al., 2016). However, the results of that study also show much stronger magnitudes of anisotropy (delay times) in the Superior craton north of the MCR, and much smaller values within and south of the MCR. Based on these lateral variations in delay times over short distances, the authors conclude that much of the azimuthal anisotropy is sourced in the lithosphere, rather than the asthenosphere. This is consistent with our Rayleigh wave observations of variations in the strength of anisotropy, which have much stronger sensitivity to lithospheric depths than asthenospheric. The variations in fast orientation observed in this study are not consistent with the shear wave splitting results, but can be explained by the differing depth sensitivities of the two measurements.

6.2.5. Sublithospheric anisotropy

It is generally assumed that within the lithosphere, alignment of minerals occurred during some major formation or deformation event and, as the rock cooled, the alignment was frozen in place. The observed fast orientation today thus represents the maximum strain at some point in the past. In the asthenosphere, present-day mantle convection is thought to align the minerals, and thus the observed fast orientation should represent present-day (or geologically recent) strain.

Several authors have used the observation of changes in anisotropy in depth to indicate the extent of the lithosphere at different periods in time (e.g., Yuan and Romanowicz, 2010). Many such comparisons are better made in depth than in frequency, and will be examined in future work. Surface wave phase velocity measurements average over some depth range, but should also present a smooth, coherent field of fast orientations representing asthenospheric flow at long periods (e.g., Montagner, 1994; Park and Levin, 2002). We note a clear change between 140 and 180 s period in the anisotropic fast orientation within the Superior craton; additionally, the magnitude of anisotropy increases with period. This indicates that a large component of the signal likely

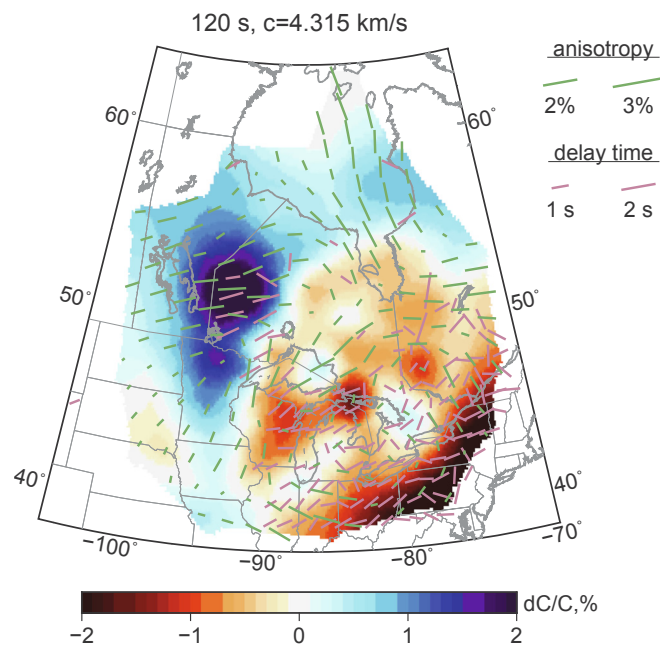


Fig. 9. Phase velocity azimuthal anisotropy at 120 s period (green bars) and SKS splitting measurements (magenta bars). SKS splits from the IRIS DMC database (DMC, 2012) are spatially averaged in 1° bins for clarity.

originates in the asthenosphere at these longer periods. A similar change in fast orientation and increase in strength of anisotropy was observed by Petrescu et al. (2017) in the eastern Canadian Shield. Given the assertion that surface wave measurements will have limited sensitivity to asthenospheric anisotropy at depths of 200 km or more (Marone and Romanowicz, 2007), which is certainly the depth range of interest beneath the thick cratonic lithosphere here, the observed magnitudes of anisotropy are likely an underestimate. A model of azimuthal anisotropy from the joint inversion of surface waveforms and SKS splitting measurements by Marone and Romanowicz (2007) approaches 2% peak-to-peak anisotropy at 300 km depth in the Superior/Great Lakes region; we observe slightly larger values in this region at the longest periods (3–4%), due to the higher resolution in this study.

Beneath the subsurface Grenville Province, at periods of 60–220 s, the fast orientation of anisotropy is consistently aligned in a NW–SE direction. This is not the same as the direction of plate motion, nor is it the strike of the orogen that formed this province (anisotropic fast directions typically parallel the strike of orogens, rather than the direction of compression). Shear wave splitting measurements do not match our observed fast-direction orientation (Fig. 9; Yuan and Romanowicz, 2010). However, in the adjacent Appalachians, the fast axis determined from receiver functions and from the top layer of a two-layer anisotropic model for shear wave splitting results determined by Yuan and Levin (2014) does match our observations, and is interpreted as a lithospheric signal. The origin is uncertain, but the authors suggest that partial lithospheric delamination is the most likely candidate. It is possible that we are observing the same lithospheric anisotropy beneath the southeasternmost Grenville.

Isotropic and anisotropic phase velocity variations thus record many episodes of formation and deformation throughout geologic history. Preservation of the Superior craton, some of the oldest crust and lithosphere on Earth, allows us to observe a velocity structure distinct from surrounding rocks that are just a billion years younger. Orogenic activity creates the strongest anisotropic signatures in the study region. Hotspot passage affects isotropic velocities, but it takes rifting with high volumes of magmatism from the MCR to most effectively destroy the anisotropic signatures.

7. Conclusions

Our high-resolution phase velocity maps of the central North American craton show strong lateral variations in isotropic and anisotropic phase velocities at all periods from 20 to 200 s. At shorter periods, the phase velocity anomalies correlate well with surface tectonic features such as the Superior craton, the Trans-Hudson Orogen, Mid-Continent Rift, and the Proterozoic orogens south and east of the Superior. At lithospheric depths, the Superior craton is characterized by high velocities, particularly in the west, and strong anisotropy with fast orientations that are E–W in the west and east, and NE–SW in the center. Relatively lower velocities in the east are likely the result of lithospheric refertilization, associated with the Great Meteor hotspot and/or previous tectonic modification. The Proterozoic orogenic belts (e.g. Trans-Hudson orogen, Yavapai, Mazatzal and Grenville) show up as moderately low-velocity anomalies at periods corresponding to crustal depths, and at least 2% slower than the Superior craton at periods ≥ 60 s. In the southeast, anisotropic fast orientations correspond to the strike of the orogenic belts, but rotate to a NW–SE orientation at ≥ 60 s period, suggesting a change in lithospheric deformation. The Mid-Continent Rift is the slowest anomaly in the study area at periods corresponding to crustal depths, and continues to show low velocities at longer periods, though the location of the slowest anomalies shifts with period. At periods ≥ 140 s, corresponding to the lowermost lithosphere and the sublithospheric mantle, the magnitude of anisotropy increases significantly and fast orientations become more homogeneous across the region, suggesting a contribution to anisotropy from asthenospheric flow. The phase velocity maps illuminate significant differences in the

structure and fabric of the Precambrian continental lithosphere across our study region, including distinct seismic signatures of Proterozoic orogenesis, lithospheric metasomatism, and modification of the North American craton by a variety of tectonic processes including major rifting events and hotspot-lithosphere interaction.

Data availability

All seismic waveform data are available from either the IRIS Data Management Center or the Canadian National Data Centre. See the [Supplementary material](#) for details of the seismograph networks used in this study.

Declaration of Competing Interest

The authors declare that they have no known competing financial interests or personal relationships that could have appeared to influence the work reported in this paper.

Acknowledgments

FD and AF are supported by the Natural Sciences and Engineering Research Council of Canada (NSERC) through the Discovery Grants and Canada Research Chair programmes [<https://doi.org/10.13039/501100000038>] (341802-2013-RGPIN). This publication represents contribution 20190346 to the Open Geoscience Program of Natural Resources Canada.

Appendix A. Supplementary data

Supplementary data associated with this article can be found, in the online version, at <https://doi.org/10.1016/j.precamres.2020.105662>.

References

- Adetunji, A.Q., Ferguson, I.J., Jones, A.G., 2015. Imaging the mantle lithosphere of the precambrian grenville province: large-scale electrical resistivity structures. *Geophys. J. Int.* 201, 1040–1061. <https://doi.org/10.1093/gji/ggv060>.
- Aulbach, S., Creaser, R.A., Stachel, T., Heaman, L.M., Chinn, I.L., Kong, J., 2018. Diamond ages from Victor (Superior Craton): intra-mantle cycling of volatiles (C, N, S) during supercontinent reorganisation. *Earth Planet. Sci. Lett.* 490, 77–87. <https://doi.org/10.1016/j.epsl.2018.03.016>.
- Babuška, V., & Plomerová, J., 1989. Seismic anisotropy of the subcrustal lithosphere in Europe: another clue to recognition of accreted terranes? In Hillhouse, J. (Ed.). *Deep Structure and Past Kinematics of Accreted Terranes*. American Geophysical Union volume 50 of Geophysical Monographs. pp. 209–217. <https://doi.org/10.1029/GM050p0209>.
- Babuška, V., Plomerová, J., 2006. European mantle lithosphere assembled from rigid microplates with inherited seismic anisotropy. *Phys. Earth Planet. Inter.* 158, 264–280. <https://doi.org/10.1016/j.pepi.2006.01.010>.
- Bastow, I., Owens, T., Helffrich, G., Knapp, J., 2007. Spatial and temporal constraints on sources of seismic anisotropy: evidence from the scottish highlands. *Geophys. Res. Lett.* 34, L05305. <https://doi.org/10.1029/2006GL028911>.
- Bédard, J.H., Harris, L.B., 2014. Neoproterozoic disaggregation and reassembly of the Superior craton. *Geology* 42, 951–954. <https://doi.org/10.1130/G35770.1>.
- Bollmann, T.A., van der Lee, S., Frederiksen, A.W., Wolin, E., Revenaugh, J., Wiens, D.A., Darbyshire, F.A., Stein, S., Wysession, M.E., Jurdy, D., 2019. P wave teleseismic traveltome tomography of the North American Midcontinent. *J. Geophys. Res.: Solid Earth* 124, 1725–1742. <https://doi.org/10.1029/2018JB016627>.
- Bourová, E., Kassaras, I., Pedersen, H., Yanovskaya, T., Hatzfeld, D., Kiratzi, A., 2005. Constraints on absolute S velocities beneath the Aegean Sea from surface wave analysis. *Geophys. J. Int.* 160, 1006–1019. <https://doi.org/10.1111/j.1365-246X.2005.02565.x>.
- Bowring, S.A., Karlstrom, K.E., 1990. Growth, stabilization, and reactivation of Proterozoic lithosphere in the southwestern United States. *Geology* 18, 1203–1206. [https://doi.org/10.1130/0091-7613\(1990\)018%3C\\$1203:GSAROP\\$>2.3.CO;2](https://doi.org/10.1130/0091-7613(1990)018%3C$1203:GSAROP$>2.3.CO;2).
- Boyce, A., Bastow, I., Darbyshire, F., Ellwood, A., Gilligan, A., Levin, V., Menke, W., 2016. Subduction beneath Laurentia modified the eastern North American cratonic edge: evidence from P wave and S wave tomography. *J. Geophys. Res.: Solid Earth* 121, 5013–5030. <https://doi.org/10.1002/2016JB012838>.
- Boyce, A., Bastow, I.D., Golos, E.M., Rondenay, S., Burdick, S., Van der Hilst, R.D., 2019. Variable modification of continental lithosphere during the Proterozoic Grenville orogeny: evidence from teleseismic P-wave tomography. *Earth Planet. Sci. Lett.* 525, 115763. <https://doi.org/10.1016/j.epsl.2019.115763>.
- Brocher, T.M., Christensen, N.I., 1990. Seismic anisotropy due to preferred mineral

- orientation observed in shallow crustal rocks in southern Alaska. *Geology* 18, 737–740. [https://doi.org/10.1130/0091-7613\(1990\)0185<\\$<0737:SADTPM\\$>2.3.CO;2](https://doi.org/10.1130/0091-7613(1990)0185<$<0737:SADTPM$>2.3.CO;2).
- Brune, J., Dorman, J., 1963. Seismic waves and Earth structure in the Canadian Shield. *Bull. Seismol. Soc. Am.* 53, 167–210.
- Burdick, S., Vernon, F.L., Martynov, V., Eakins, J., Cox, T., Tytell, J., Mulder, T., White, M.C., Astiz, L., Pavlis, G.L., et al., 2017. Model update May 2016: upper-mantle heterogeneity beneath North America from travel-time tomography with global and USArray data. *Seismol. Res. Lett.* 88, 319–325. <https://doi.org/10.1785/0220160186>.
- Bystricky, M., Kunze, K., Burlini, L., Burg, J.-P., 2000. High shear strain of olivine aggregates: rheological and seismic consequences. *Science* 290, 1564–1567. <https://doi.org/10.1126/science.290.5496.1564>.
- Canil, D., 2008. Canada's craton: a bottoms-up view. *GSA Today* 18, 4–10. <https://doi.org/10.1130/GSAT01806A.1>.
- Clowes, R., 2010. Initiation, development, and benefits of Lithoprobe—shaping the direction of Earth science in Canada and beyond. *Can. J. Earth Sci.* 47, 291–314. <https://doi.org/10.1139/E09-074>.
- Corrigan, D., Pehrsson, S., Wodicka, N., de Kemp, E., 2009. The Paleoproterozoic Trans-Hudson Orogen: a prototype of modern accretionary processes. *Geol. Soc. London Spec. Publ.* 327, 457–479. <https://doi.org/10.1144/SP327.19>.
- Corrigan, H., Hamner, S., 1997. Anorthositic and related granitoids in the Grenville orogen: a product of convective thinning of the lithosphere? *Geology* 25, 61–64. [https://doi.org/10.1130/0091-7613\(1997\)0255<\\$<0061:AARGITS\\$>2.3.CO;2](https://doi.org/10.1130/0091-7613(1997)0255<$<0061:AARGITS$>2.3.CO;2).
- Dalton, C.A., Gaherty, J.B., 2013. Seismic anisotropy in the continental crust of northwestern Canada. *Tectonics* 36, 1633–1659. <https://doi.org/10.1002/2017TC004479>.
- Darbyshire, F., Bastow, I., Petrescu, L., Gilligan, A., Thompson, D., 2017. A tale of two orogens: crustal processes in the Proterozoic Trans-Hudson and Grenville Orogens, eastern Canada. *Tectonics* 36, 1633–1659. <https://doi.org/10.1002/2017TC004479>.
- Darbyshire, F.A., Eaton, D.W., Bastow, I.D., 2013. Seismic imaging of the lithosphere beneath Hudson Bay: episodic growth of the Laurentian mantle keel. *Earth Planet. Sci. Lett.* 373, 179–193. <https://doi.org/10.1016/j.epsl.2013.05.002>.
- Darbyshire, F.A., Eaton, D.W., Frederiksen, A.W., Ertolahti, L., 2007. New insights into the lithosphere beneath the Superior Province from Rayleigh wave dispersion and receiver function analysis. *Geophys. J. Int.* 169, 1043–1068. <https://doi.org/10.1111/j.1365-246X.2006.03259.x>.
- Darbyshire, F.A., Lebedev, S., 2009. Rayleigh wave phase-velocity heterogeneity and multilayered azimuthal anisotropy of the Superior Craton, Ontario. *Geophys. J. Int.* 176, 215–234. <https://doi.org/10.1111/j.1365-246X.2008.03982.x>.
- DMC, I., 2012. Data Services Products: SWS-DBs Shear-wave splitting databases. <https://doi.org/10.17611/DP/SWS.1>.
- Eaton, D., Darbyshire, F., 2010. Lithospheric architecture and crustal evolution of the Hudson Bay region. *Tectonophysics* 480, 1–22. <https://doi.org/10.1016/j.tecto.2009.09.006>.
- Eaton, D.W., Frederiksen, A., 2007. Seismic evidence for convection-driven motion of the North American plate. *Nature* 446, 428–431. <https://doi.org/10.1038/nature05675>.
- Ernst, R., Bleeker, W., 2010. Large igneous provinces (LIPs), giant dyke swarms, and mantle plumes: significance for breakup events within Canada and adjacent regions from 2.5 Ga to the Present. *Can. J. Earth Sci.* 47, 695–739. <https://doi.org/10.1139/E10-025>.
- Ferré, E.C., Gëbelin, A., Conder, J.A., Christensen, N., Wood, J.D., Teyssier, C., 2014. Seismic anisotropy of the Archean crust in the Minnesota River Valley, Superior Province. *Geophys. Res. Lett.* 41, 1514–1522. <https://doi.org/10.1002/2013GL059116>.
- Forsyth, D., Li, A., 2005. Array analysis of two-dimensional variations in surface wave velocity and azimuthal anisotropy in the presence of multipathing interference. In: Levander, A., Nolet, G., (Eds.). *Seismic Earth: Array Analysis of Broadband Seismograms*. Washington, D.C.: American Geophysical Union volume 157 of Geophysical Monograph Series. <https://doi.org/10.1029/157GM06>.
- Foster, A., Ekström, G., Nettles, M., 2014. Surface wave phase velocities of the Western United States from a two-station method. *Geophys. J. Int.* 196, 1189–1206. <https://doi.org/10.1093/gji/ggt454>.
- Frederiksen, A., Bollmann, T., Darbyshire, F., van der Lee, S., 2013. Modification of continental lithosphere by tectonic processes: a tomographic image of central North America. *J. Geophys. Res.: Solid Earth* 118, 1051–1066. <https://doi.org/10.1002/jgrb.50060>.
- Frederiksen, A., Deniset, I., Ola, O., Toni, D., 2013. Lithospheric fabric variations in central North America: influence of rifting and Archean tectonic styles. *Geophys. Res. Lett.* 40, 4583–4587. <https://doi.org/10.1002/grl.50879>.
- Frederiksen, A., Miong, S.-K., Darbyshire, F., Eaton, D., Rondenay, S., Sol, S., 2007. Lithospheric variations across the Superior Province, Ontario, Canada: evidence from tomography and shear wave splitting. *J. Geophys. Res.: Solid Earth* 112, B07318. <https://doi.org/10.1029/2006JB004861>.
- Friederich, W., 1998. Wave-theoretical inversion of teleseismic surface waves in a regional network: phase velocity maps and a 3-D upper mantle shear wave velocity model for southern Germany. *Geophys. J. Int.* 132, 203–225. <https://doi.org/10.1046/j.1365-246x.1998.00425.x>.
- Gaherty, J.B., 2004. A surface wave analysis of seismic anisotropy beneath eastern North America. *Geophys. J. Int.* 158, 1053–1066. <https://doi.org/10.1111/j.1365-246X.2004.02371.x>.
- Gilligan, A., Bastow, I.D., Darbyshire, F.A., 2016. Seismological structure of the 1.8 Ga Trans-Hudson Orogen of North America. *Geochim. Geophys. Geosyst.* 17, 2421–2433. <https://doi.org/10.1002/2016GC006419>.
- Golos, E., Fang, H., Yao, H., Zhang, H., Burdick, S., Vernon, F., Schaeffer, A., Lebedev, S., van der Hilst, R., 2018. Shear wave tomography beneath the United States using a joint inversion of surface and body waves. *J. Geophys. Res.: Solid Earth* 123, 5169–5189. <https://doi.org/10.1029/2017JB014894>.
- Gomberg, J., Priestley, K., Masters, T., Brune, J., 1988. The structure of the crust and upper mantle of northern Mexico. *Geophys. J. Int.* 94, 1–20.
- Green, A.G., Cannon, W., Milkereit, B., Hutchinson, D., Davidson, A., Behrendt, J., Spencer, C., Lee, M., Morel-à L'Huissier, P., Agena, W., 1989. A “Glimpce” of the Deep Crust Beneath the Great Lakes. In: R. Mereu, S. Mueller, & D. Fountain (Eds.), *Properties and Processes of Earth's Lower Crust*. American Geophysical Union volume 51 of Geophysical Monograph Series. pp. 65–80. <https://doi.org/10.1029/GM051p0065>.
- Gripp, A., Gordon, R., 2002. Young tracks of hotspots and current plate velocities. *Geophys. J. Int.* 150, 321–361.
- Groulier, P.-A., Indares, A., Dunning, G., Moukhsil, A., Jenner, G., 2018. Syn-orogenic magmatism over 100 m.y. in high crustal levels of the central Grenville Province: characteristics, age and tectonic significance. *Lithos* 312–313, 128–152. <https://doi.org/10.1016/j.lithos.2018.04.025>.
- Hammer, P.T., Clowes, R.M., Cook, F.A., van der Velden, A.J., Vasudevan, K., 2010. The Lithoprobe trans-continental lithospheric cross sections: imaging the internal structure of the North American continent. *Can. J. Earth Sci.* 47, 821–857. <https://doi.org/10.1139/E10-036>.
- Hanmer, S., Corrigan, D., Pehrsson, S., Nadeau, L., 2000. SW Grenville Province, Canada: the case against post-1.4 Ga accretionary tectonics. *Tectonophysics* 319, 33–51. [https://doi.org/10.1016/S0040-1951\(99\)00317-0](https://doi.org/10.1016/S0040-1951(99)00317-0).
- Hart, T.R., MacDonald, C.A., 2007. Proterozoic and Archean geology of the Nipigon Embayment: implications for emplacement of the Mesoproterozoic Nipigon diabase sills and mafic to ultramafic intrusions. *Can. J. Earth Sci.* 44, 1021–1040. <https://doi.org/10.1139/e07-026>.
- Heaman, L., Kjarsgaard, B., 2000. Timing of eastern North American kimberlite magmatism: continental extension of the Great Meteor hotspot track? *Earth Planet. Sci. Lett.* 178, 253–268. [https://doi.org/10.1016/S0012-821X\(00\)00790-0](https://doi.org/10.1016/S0012-821X(00)00790-0).
- Heaman, L., Kjarsgaard, B., Creaser, R., 2004. The temporal evolution of North American kimberlites. *Lithos* 76, 377–397. <https://doi.org/10.1016/j.lithos.2004.03.047>.
- Heaman, L., Moser, D., 1997. Proterozoic zircon growth in Archean lower crustal xenoliths, southern Superior craton – a consequence of Matachewan ocean opening. *Contrib. Miner. Petrol.* 128, 164–175. <https://doi.org/10.1007/s004100050301>.
- Herrmann, R.B., 2013. Computer programs in seismology: an evolving tool for instruction and research. *Seismol. Res. Lett.* 84, 1081–1088. <https://doi.org/10.1785/0220110096>.
- Hollings, P., Fralick, P., Kissin, S., 2004. Geochemistry and geodynamic implications of the Mesoproterozoic English Bay granite rhyolite complex, northwestern Ontario. *Can. J. Earth Sci.* 41, 1329–1338. <https://doi.org/10.1139/e04-077>.
- Hynes, A., Rivers, T., 2010. Protracted continental collision – evidence from the Grenville Orogen. *Can. J. Earth Sci.* 47, 591–620. <https://doi.org/10.1139/E10-003>.
- James, D., Assumpção, M., 1996. Tectonic implications of S-wave anisotropy beneath SE Brazil. *Geophys. J. Int.* 126, 1–10. <https://doi.org/10.1111/j.1365-246X.1996.tb05263.x>.
- Jaupart, C., Mareschal, J.-C., Bouquerel, H., Phaneuf, C., 2014. The building and stabilization of an Archean Craton in the Superior Province, Canada, from a heat flow perspective. *J. Geophys. Res.: Solid Earth* 119, 9130–9155. <https://doi.org/10.1002/2014JB011018>.
- Jordan, T., 1988. Structure and formation of the continental tectosphere. *J. Petrol. (Special Lithosphere Issue)* 1, 11–37.
- Karato, S.-I., Jung, H., Katayama, I., Skemer, P., 2008. Geodynamic significance of seismic anisotropy of the upper mantle: new insights from laboratory studies. *Annu. Rev. Earth Planet. Sci.* 36, 59–95. <https://doi.org/10.1146/annurev.earth.36.031207.124120>.
- Kay, I., Sol, S., Kendall, J.-M., Thomson, C., White, D., Asudeh, I., Roberts, B., Francis, D., 1999. Shear wave splitting observations in the Archean craton of Western Superior. *Geophys. Res. Lett.* 26, 2669–2672. <https://doi.org/10.1029/1999GL010493>.
- Keller, G., Karlstrom, K., Williams, M., Miller, K., Andronico, C., Levander, A., Snelson, C., Prodehl, C., 2005. The dynamic nature of the continental crust-mantle boundary: Crustal evolution in the southern Rocky mountain region as an example. In: K. Karlstrom, & G. Keller (Eds.), *The Rocky Mountain region—An evolving lithosphere: Tectonics, geochemistry, and geophysics*. American Geophysical Union volume 154 of Geophysical Monograph Series. pp. 403–420. <https://doi.org/10.1029/154GM30>.
- Kennett, B., Engdahl, E., Buland, R., 1995. Constraints on seismic velocities in the earth from travel times. *Geophys. J. Int.* 122, 108–124. <https://doi.org/10.1111/j.1365-246X.1995.tb03540.x>.
- King, S.D., 2005. Archean cratons and mantle dynamics. *Earth Planet. Sci. Lett.* 234, 1–14. <https://doi.org/10.1016/j.epsl.2005.03.007>.
- Knopoff, L., Muller, S., Pilant, W., 1966. Structure of the crust and upper mantle in the Alps from the phase velocity of Rayleigh waves. *Bull. Seismol. Soc. Am.* 56, 1009–1044.
- Korenaga, J., 2006. Archean geodynamics and the thermal evolution of the earth. In: K. Benn, J. Mareschal, & K. Condie (Eds.), *Archean Geodynamics and Environments: Geophysical Monograph*. American Geophysical Union. vol. 164. pp. 7–33. <https://doi.org/10.1029/164GM03>.
- Langford, F., Morin, J., 1976. The development of the Superior Province of northwestern Ontario by merging island arcs. *Am. J. Sci.* 276, 1023–1034.
- Lebedev, S., van der Hilst, R., 2008. Global upper-mantle tomography with the automated multimode inversion of surface and S wave forms. *Geophys. J. Int.* 173, 505–518. <https://doi.org/10.1111/j.1365-246X.2008.03721.x>.
- Lee, C., Luffi, P., Chin, E., 2011. Building and destroying continental mantle. *Annu. Rev. Earth Planet. Sci.* 39, 59–90. <https://doi.org/10.1146/annurev-earth-040610-133505>.
- Liang, C., Langston, C.A., 2009. Wave gradiometry for USArray: Rayleigh waves. *J. Geophys. Res.: Solid Earth* 114, B02308. <https://doi.org/10.1029/2008JB005918>.

- Lin, F.-C., Ritzwoller, M.H., Sneider, R., 2009. Eikonal tomography: surface wave tomography by phase front tracking across a regional broad-band seismic array. *Geophys. J. Int.* 177, 1091–1110. <https://doi.org/10.1111/j.1365-246X.2009.04105.x>.
- Ludden, J., Hynes, A., 2000. The Lithoprobe Abitibi-Grenville transect: two billion years of crust formation and recycling in the Precambrian Shield of Canada. *Can. J. Earth Sci.* 37, 459–476. <https://doi.org/10.1139/e99-120>.
- Mareschal, J., Jaupart, C., 2004. Variations of surface heat flow and lithospheric thermal structure beneath the North American craton. *Earth Planet. Sci. Lett.* 223, 65–77. <https://doi.org/10.1016/j.epsl.2004.04.002>.
- Mareschal, J., Jaupart, C., Rolandone, F., Gariépy, C., Fowler, C., Bienfait, G., Carbonne, C., Lapointe, R., 2005. Heat flow, thermal regime, and elastic thickness of the lithosphere in the Trans-Hudson Orogen. *Can. J. Earth Sci.* 42, 517–532. <https://doi.org/10.1139/E04-088>.
- Marone, F., Romanowicz, B., 2007. The depth distribution of azimuthal anisotropy in the continental upper mantle. *Nature* 447, 198–201. <https://doi.org/10.1038/nature05742>.
- Meier, T., Dietrich, B., Stockhert, B., Harjes, H.-P., 2004. One-dimensional models of shear wave velocity for the eastern Mediterranean obtained from the inversion of Rayleigh wave phase velocities and tectonic implications. *Geophys. J. Int.* 156, 45–58. <https://doi.org/10.1111/j.1365-246X.2004.02121.x>.
- Meltzer, A., Christensen, N., 2001. Nanga Parbat crustal anisotropy: implications for interpretation of crustal velocity structure and shear wave splitting. *Geophys. Res. Lett.* 28, 2129–2132. <https://doi.org/10.1029/2000GL012262>.
- Montagner, J.-P., 1994. Can seismology tell us anything about convection in the mantle? *Rev. Geophys.* 32, 115–137. <https://doi.org/10.1029/94RG00099>.
- Montagner, J.-P., Anderson, D.L., 1989. Petrological constraints on seismic anisotropy. *Phys. Earth Planet. Inter.* 54, 82–105. [https://doi.org/10.1016/0031-9201\(89\)90189-1](https://doi.org/10.1016/0031-9201(89)90189-1).
- Musacchio, G., White, D.J., Asudeh, I., Thomson, C., 2004. Lithospheric structure and composition of the Archean western Superior Province from seismic refraction/wide-angle reflection and gravity modeling. *J. Geophys. Res.* 109, B03304. <https://doi.org/10.1029/2003JB002427>.
- Nishimura, C.E., Forsyth, D.W., 1989. The anisotropic structure of the upper mantle in the Pacific. *Geophys. J. Int.* 96, 203–229.
- Ojakangas, R., Morey, G., Green, J., 2001. The Mesoproterozoic Midcontinent Rift System, Lake Superior Region, USA. *Sed. Geol.* 141–142, 421–442. [https://doi.org/10.1016/S0037-0738\(01\)00085-9](https://doi.org/10.1016/S0037-0738(01)00085-9).
- Ola, O., Frederiksen, A., Bollmann, T., van der Lee, S., Darbyshire, F., Wolin, E., Revenaugh, J., Stein, C., Stein, S., Wyssession, M., 2016. Anisotropic zonation in the lithosphere of Central North America: Influence of a strong cratonic lithosphere on the Mid-Continent Rift. *Tectonophysics* 683, 367–381. <https://doi.org/10.1016/j.tecto.2016.06.031>.
- Paige, C., Saunders, M., 1982. LSQR: an algorithm for sparse linear equations and sparse least squares. *Assoc. Comput. Mach. Trans. Math. Software* 8, 43–71.
- Park, J., Levin, V., 2002. Seismic anisotropy: tracing plate dynamics in the Mantle. *Science* 296, 485–489. <https://doi.org/10.1126/science.1067319>.
- Pawlak, A., Eaton, D.W., Darbyshire, F., Lebedev, S., Bastow, I.D., 2012. Crustal anisotropy beneath Hudson Bay from ambient noise tomography: evidence for post-orogenic lower-crustal flow? *J. Geophys. Res.: Solid Earth* 117, B08301. <https://doi.org/10.1029/2011JB009066>.
- Percival, J., 2007. Geology and metallogeny of the Superior Province, Canada. In W. Goodfellow (Ed.), *Mineral deposits of Canada: a synthesis of major deposit-types, district metallogeny, the evolution of geological provinces and exploration methods*, Geol. Assoc. Can., Mineral Deposits Division, Spec. Pub. vol. 5. pp. 903–928.
- Percival, J., Sanborn-Barrie, M., Skulski, T., Stott, G., Helmstaedt, H., White, D., 2006. Tectonic evolution of the western Superior Province from NATMAP and Lithoprobe studies. *Can. J. Earth Sci.* 43, 1085–1117. <https://doi.org/10.1139/e06-062>.
- Perry, C., Rosieanu, C., Mareschal, J.-C., Jaupart, C., 2010. Thermal regime of the lithosphere in the Canadian Shield. *Can. J. Earth Sci.* 47, 389–408. <https://doi.org/10.1139/E09-059>.
- Petrescu, L., Bastow, I., Darbyshire, F., Gilligan, A., Bodin, T., Menke, W., Levin, V., 2016. Three billion years of crustal evolution in eastern Canada: constraints from receiver functions. *J. Geophys. Res.: Solid Earth* 121, 788–811. <https://doi.org/10.1002/2015JB012348>.
- Petrescu, L., Darbyshire, F., Bastow, I., Totten, E., Gilligan, A., 2017. Seismic anisotropy of Precambrian lithosphere: insights from Rayleigh wave tomography of the eastern Superior Craton. *J. Geophys. Res.: Solid Earth* 122, 3754–3775. <https://doi.org/10.1002/2016JB013599>.
- Plomerová, J., Kouba, D., Babuška, V., 2002. Mapping the lithosphere-asthenosphere boundary through changes in surface-wave anisotropy. *Tectonophysics* 358, 175–185. [https://doi.org/10.1016/S0040-1951\(02\)00423-7](https://doi.org/10.1016/S0040-1951(02)00423-7).
- Pollitz, F., Mooney, W., 2016. Seismic velocity structure of the crust and shallow mantle of the Central and Eastern United States by seismic surface wave imaging. *Geophys. Res. Lett.* 43, 118–126. <https://doi.org/10.1002/2016JB013599>.
- Priestley, K., McKenzie, D., Ho, T., 2019. A lithosphere-asthenosphere boundary - a global model derived from multimode surface-wave tomography and petrology. In H. Yuan, & B. Romanowicz (Eds.), *Lithospheric Discontinuities: Geophysical Monographs chapter 6*. American Geophysical Union volume 239. pp. 111–123. <https://doi.org/10.1002/9781119249740.ch6>.
- Rivers, T., 2015. Tectonic setting and evolution of the Grenville orogen: an assessment of progress over the last 40 years. *Geosci. Can.* 42, 77–123. <https://doi.org/10.12789/geocanj.2014.41.057>.
- Rivers, T., Corrigan, D., 2000. Convergent margin on southeastern Laurentia during the Mesoproterozoic: tectonic implications. *Can. J. Earth Sci.* 37, 359–383. <https://doi.org/10.1139/e99-067>.
- Rondenay, S., Bostock, M.G., Hearn, T.M., White, D.J., Ellis, R.M., 2000. Lithospheric assembly and modification of the SE Canadian Shield: Abitibi-Grenville teleseismic experiment. *J. Geophys. Res.: Solid Earth* 105, 13735–13754. <https://doi.org/10.1029/2000JB900022>.
- Rychert, C.A., Shearer, P.M., 2009. A global view of the lithosphere-asthenosphere boundary. *Science* 324, 495–498. <https://doi.org/10.1126/science.1169754>.
- Sato, Y., 1955. Analysis of dispersed surface waves by means of Fourier Transform I. *Bull. Earthq. Res. Inst. Tokyo University* 33, 33–48.
- Schaeffer, A., Lebedev, S., 2014. Imaging the North American continent using waveform inversion of global and USArray data. *Earth Planet. Sci. Lett.* 402, 26–41. <https://doi.org/10.1016/j.epsl.2014.05.014>.
- Schaeffer, A., Lebedev, S., Becker, T., 2016. Azimuthal seismic anisotropy in the Earth's upper mantle and the thickness of tectonic plates. *Geophys. J. Int.* 207, 901–933. <https://doi.org/10.1093/gji/ggw309>.
- Schmandt, B., Lin, F.-C., 2014. P and S wave tomography of the mantle beneath the United States. *Geophys. Res. Lett.* 41, 6342–6349. <https://doi.org/10.1002/2014GL061231>.
- Schneider, D., Heizler, M., Bickford, M., Wortman, G., Condie, K., Perilli, S., 2007. Timing constraints of orogeny to cratonization: Thermochronology of the Paleoproterozoic Trans-Hudson orogen, Manitoba and Saskatchewan, Canada. *Precamb. Res.* 153, 65–95. <https://doi.org/10.1016/j.precambres.2006.11.007>.
- Schutt, D.L., Leshner, C.E., 2010. Compositional trends among Kaapvaal Craton garnet peridotite xenoliths and their effects on seismic velocity and density. *Earth Planet. Sci. Lett.* 300, 367–373. <https://doi.org/10.1016/j.epsl.2010.10.018>.
- Shen, W., Ritzwoller, M.H., 2016. Crustal and uppermost mantle structure beneath the United States. *J. Geophys. Res.: Solid Earth* 121, 4306–4342. <https://doi.org/10.1002/2016JB012887>.
- Shen, W., Ritzwoller, M.H., Schulte-Pelkum, V., 2013. Crustal and uppermost mantle structure in the central US encompassing the Midcontinent Rift. *J. Geophys. Res.: Solid Earth* 118, 4325–4344. <https://doi.org/10.1002/jgrb.50321>.
- Silver, P., Chan, W., 1988. Implications for continental structure and evolution from seismic anisotropy. *Nature* 335, 34–39. <https://doi.org/10.1038/335034a0>.
- Silver, P.G., Chan, W.W., 1991. Shear wave splitting and subcontinental mantle deformation. *J. Geophys. Res.: Solid Earth* 96, 16429–16454. <https://doi.org/10.1029/91JB00899>.
- Silver, P.G., Kaneshima, S., 1993. Constraints on mantle anisotropy beneath Precambrian North America from a transportable teleseismic experiment. *Geophys. Res. Lett.* 20, 1127–1130. <https://doi.org/10.1029/93GL00775>.
- Sleep, N., 1990. Monteregian hotspot track: a long-lived mantle plume. *J. Geophys. Res.: Solid Earth* 95, 21983–21990.
- Smit, K., Stachel, T., Stern, R., 2014. Diamonds in the Attawapiskat area of the Superior craton (Canada): evidence for a major diamond-forming event younger than 1.1Ga. *Contrib. Mineral. Petrol.* 167, 1–16. <https://doi.org/10.1007/s00410-013-0962-6>.
- Smith, M., Dahlen, F., 1973. The azimuthal dependence of Love and Rayleigh wave propagation in a slightly anisotropic medium. *J. Geophys. Res.* 78, 3321–3333.
- Sol, S., Thomson, C., Kendall, J.-M., White, D., VanDecar, J., Asudeh, I., 2002. Seismic tomographic images of the cratonic upper mantle beneath the Western Superior Province of the Canadian Shield—a remnant Archean slab? *Phys. Earth Planet. Inter.* 134, 53–69. [https://doi.org/10.1016/S0031-9201\(02\)00081-X](https://doi.org/10.1016/S0031-9201(02)00081-X).
- St-Onge, M.R., Searle, M.P., Wodicka, N., 2006. Trans-Hudson Orogen of North America and Himalaya-Karakoram-Tibetan Orogen of Asia: structural and thermal characteristics of the lower and upper plates. *Tectonics* 25, TC4006. <https://doi.org/10.1029/2005TC001907>.
- Stein, C.A., Kley, J., Stein, S., Hindle, D., Keller, G.R., 2015. North America's Midcontinent Rift: when rift met LIP. *Geosphere* 11, 1607–1618. <https://doi.org/10.1130/GES01183.1>.
- Stein, C.A., Stein, S., Merino, M., Keller, G.R., Flesch, L.M., Jurdy, D.M., 2014. Was the Midcontinent Rift part of a successful seafloor-spreading episode? *Geophys. Res. Lett.* 41, 1465–1470. <https://doi.org/10.1002/2013GL059176>.
- Stein, S., Stein, C.A., Elling, R., Kley, J., Keller, G.R., Wyssession, M., Rooney, T., Frederiksen, A., Moucha, R., 2018. Insights from North America's failed Midcontinent Rift into the evolution of continental rifts and passive continental margins. *Tectonophysics* 744, 403–421. <https://doi.org/10.1016/j.tecto.2018.07.021>.
- Sutcliffe, R., 1991. Proterozoic geology of the Lake Superior area. In P. Thurston, H. Williams, R. Sutcliffe, & G. Stott (Eds.), *Geology of Ontario. Ontario Geological Survey, Toronto volume 4 of Ontario Geological Survey Special Volume*. pp. 627–658.
- Thurston, P., 1991. Proterozoic geology of Ontario: Introduction. In P. Thurston, H. Williams, R. Sutcliffe, & G. Stott (Eds.), *Geology of Ontario. Ontario Geological Survey, Toronto volume 4 of Ontario Geological Survey Special Volume*. pp. 543–546.
- Tommasi, A., Godard, M., Coromina, G., Dautria, J.-M., Barszcz, H., 2004. Seismic anisotropy and compositionally induced velocity anomalies in the lithosphere above mantle plumes: a petrological and microstructural study of mantle xenoliths from French Polynesia. *Earth Planet. Sci. Lett.* 227, 539–556. <https://doi.org/10.1016/j.epsl.2004.09.019>.
- Tommasi, A., Mainprize, D., Canova, G., Chastel, Y., 2000. Viscoplastic self-consistent and equilibrium-based modeling of olivine lattice preferred orientations: Implications for the upper mantle seismic anisotropy. *J. Geophys. Res.: Solid Earth* 105, 7893–7908. <https://doi.org/10.1029/1999JB900411>.
- Van Schmus, W., Hinze, W., 1985. The midcontinent rift system. *Annu. Rev. Earth Planet. Sci.* 13, 345–383.
- Vaucher, A., Dineur, F., Rudnick, R., 2005. Microstructure, texture and seismic anisotropy of the lithospheric mantle above a mantle plume: insights from the Labait volcano xenoliths (Tanzania). *Earth Planet. Sci. Lett.* 232, 295–314. <https://doi.org/10.1016/j.epsl.2005.01.024>.
- Vaucher, A., Nicolas, A., 1991. Mountain building: strike-parallel motion and mantle

- anisotropy. *Tectonophysics* 185, 183–201. [https://doi.org/10.1016/0040-1951\(91\)90443-V](https://doi.org/10.1016/0040-1951(91)90443-V).
- Villemaire, M., Darbyshire, F., Bastow, I., 2012. P-wave tomography of eastern North America: Evidence for mantle evolution from Archean to Phanerozoic, and modification during subsequent hot spot tectonism. *J. Geophys. Res.: Solid Earth* 117, B12302. <https://doi.org/10.1029/2012JB009639>.
- Vinnik, L., Green, R., Nicolaysen, L., 1995. Recent deformations of the deep continental root beneath southern Africa. *Nature* 375, 50–52.
- Vinnik, L., Kind, R., Kosarev, G., Makeyeva, L., 1989. Azimuthal anisotropy in the lithosphere from observations of long-period S-waves. *Geophys. J. Int.* 99, 549–559. <https://doi.org/10.1111/j.1365-246X.1989.tb02039.x>.
- Wagner, L.S., Anderson, M.L., Jackson, J.M., Beck, S.L., Zandt, G., 2008. Seismic evidence for orthopyroxene enrichment in the continental lithosphere. *Geology* 36, 935–938. <https://doi.org/10.1130/G25108A.1>.
- Wang, Z., Dahlen, F., 1995. Spherical-spline parameterization of 3-dimensional earth models. *Geophys. Res. Lett.* 22, 3099–3102.
- White, D., Zwanzig, H., Hajnal, Z., 2000. Crustal suture preserved in the Paleoproterozoic Trans-Hudson orogen, Canada. *Geology* 28, 527–530. [https://doi.org/10.1130/0091-7613\(2000\)28<\\$527:CSPITP\\$>\\$2.0.CO;2](https://doi.org/10.1130/0091-7613(2000)28<$527:CSPITP$>$2.0.CO;2).
- Whitmeyer, S.J., Karlstrom, K.E., 2007. Tectonic model for the Proterozoic growth of North America. *Geosphere* 3, 220–259. <https://doi.org/10.1130/GES00055.1>.
- Yang, B.B., Gao, S.S., Liu, K.H., Elsheikh, A.A., Lemnifi, A.A., Refayee, H.A., Yu, Y., 2014. Seismic anisotropy and mantle flow beneath the northern Great Plains of North America. *J. Geophys. Res.: Solid Earth* 119, 1971–1985. <https://doi.org/10.1002/2013JB010561>.
- Yang, B.B., Liu, Y., Dahm, H., Liu, K.H., Gao, S.S., 2017. Seismic azimuthal anisotropy beneath the eastern United States and its geodynamic implications. *Geophys. Res. Lett.* 44, 2670–2678. <https://doi.org/10.1002/2016GL071227>.
- Yao, H., van Der Hilst, R.D., de Hoop, M.V., 2006. Surface-wave array tomography in SE Tibet from ambient seismic noise and two-station analysis – I. Phase velocity maps. *Geophys. J. Int.* 166, 732–744. <https://doi.org/10.1111/j.1365-246X.2006.03028.x>.
- Yuan, H., French, S., Cupillard, P., Romanowicz, B., 2014. Lithospheric expression of geological units in central and eastern North America from full waveform tomography. *Earth Planet. Sci. Lett.* 402, 176–186. <https://doi.org/10.1016/j.epsl.2013.11.057>.
- Yuan, H., Levin, V., 2014. Stratified seismic anisotropy and the lithosphere-asthenosphere boundary beneath eastern North America. *J. Geophys. Res.: Solid Earth* 119, 3096–3114. <https://doi.org/10.1002/2013JB010785>.
- Yuan, H., Romanowicz, B., 2010. Lithospheric layering in the North American craton. *Nature* 466, 1063–1069. <https://doi.org/10.1038/nature09332>.
- Yuan, H., Romanowicz, B., Fischer, K.M., Abt, D., 2011. 3-D shear wave radially and azimuthally anisotropic velocity model of the North American upper mantle. *Geophys. J. Int.* 184, 1237–1260. <https://doi.org/10.1111/j.1365-246X.2010.04901.x>.
- Zelt, B., Ellis, R., 1999. Receiver-function studies in the Trans-Hudson Orogen, Saskatchewan. *Can. J. Earth Sci.* 36, 585–603. <https://doi.org/10.1139/e98-109>.
- Zhang, H., van der Lee, S., Wolin, E., Bollmann, T.A., Revenaugh, J., Wiens, D.A., Frederiksen, A.W., Darbyshire, F.A., Aleqabi, G., Wysession, M.E., Stein, S., Jurdy, D.M., 2016. Distinct crustal structure of the North American Midcontinent Rift from P wave receiver functions. *J. Geophys. Res.: Solid Earth* 121, 8136–8153. <https://doi.org/10.1002/2016JB013244>.
- Zhang, S., Karato, S.-I., 1995. Lattice preferred orientation of olivine aggregates deformed in simple shear. *Nature* 375, 774–777. <https://doi.org/10.1038/375774a0>.